Article

Dynamic forces shape the survival fate of eliminated cells

Lakshmi Balasubramaniam [1,2,10], Siavash Monfared [3,10],
Aleksandra Ardaševa [3], Carine Rosse [1,4], Andreas Schoenit [1], Tien Dang[1],
Chrystelle Maric [1], Mathieu Hautefeuille [5], Leyla Kocgozlu[6],
Ranjith Chilupuri[1], Sushil Dubey [1], Elisabetta Marangoni[7], Bryant L. Doss[6],
Philippe Chavrier [4], René-Marc Mége [1] ✉, Amin Doostmohammadi [3] ✉ &
Benoit Ladoux [1,8,9] ✉

Tissues eliminate unfit, unwanted or unnecessary cells through cell extrusion, and this can lead to the elimination of both apoptotic and live cells. However, the mechanical signatures that influence the fate of extruding cells remain unknown. Here we show that modified force transmission across adherens junctions inhibits apoptotic cell eliminations. By combining cell experiments with varying levels of E-cadherin junctions and three-dimensional modelling of cell monolayers, we find that these changes not only affect the fate of the extruded cells but also shift extrusion from the apical to the basal side, leading to cell invasion into soft collagen gels. We generalize our findings using xenografts and cysts cultured in matrigel, derived from patients with breast cancer. Our results link intercellular force transmission regulated by cell–cell communication to cell extrusion mechanisms, with potential implications during morphogenesis and invasion of cancer cells.

Cell extrusion is a checkpoint mechanism by which unwanted or dead cells are eliminated from a monolayer through cooperation of neighbouring cells mediated by either actomyosin contractile rings or lamellipodial protrusions[1–5]. Elimination of cells is critical for regulating cell numbers, sculpting tissues and eliminating damaged cells throughout developmental programs[6–9]. During cell extrusion, a cell within an epithelial monolayer is eliminated by its neighbours through loss of apico-basal polarization into the basal or luminal side, respectively[10,11]. Importantly, cells can be extruded alive or as dead cells[6,12,13]. The extrusion of live or dead cells has been reported during apoptosis[14], epithelial–mesenchymal transition (EMT)[15] and cancer cell invasion[16]. This makes cell extrusion a key regulator of homeostatic

pressure, which is the pressure at which cell extrusion compensates cell division[17], morphogenesis[9] and tumour progression[7]. A large variety of biochemical and biophysical cues including crowding, apoptotic stimuli and mechanical forces can thus alter the fate of these extruding cells[6,12,13,18,19]. Furthermore, the extrusion of live cells is often associated with a switch from apical to basal direction, leading to tumour cell escape and extracellular matrix invasion[10,11]. Investigating how the fate of extruding cells is orchestrated offers key clues for revealing physiological and pathological processes that remain poorly understood.

Several studies have established that cell extrusion is linked to the remodelling of neighbouring cells through compensatory proliferation[12,20–22], generation of mechanical forces[8,9,23,24], emergence

[1]Université Paris Cité, CNRS, Institut Jacques Monod, Paris, France. [2]Wellcome/Cancer Research UK Gurdon Institute, Cambridge, UK. [3]Niels Bohr Institute, University of Copenhagen, Copenhagen, Denmark. [4]Institut Curie, Paris Université Sciences et Lettres, Sorbonne Université, CNRS, UMR144, Paris, France. [5]Laboratoire de Biologie du Développement (UMR 7622), Institut de Biologie Paris Seine, Paris, France. [6]Mechanobiology Institute, National University of Singapore, Singapore, Singapore. [7]Translational Research Department, Institut Curie, PSL Research University, Paris, France. [8]Department of Physics, Friedrich-Alexander Universität Erlangen-Nürnberg, Erlangen, Germany. [9]Max-Planck-Zentrum für Physik und Medizin, Erlangen, Germany. [10]These authors contributed equally: Lakshmi Balasubramaniam, Siavash Monfared. ✉e-mail: rene-marc.mege@ijm.fr; doostmohammadi@nbi.ku.dk; benoit.ladoux@ijm.fr

of topological defects[18] and the activation of signalling pathways[25,26]. This communication between an extruding cell and its neighbours crucially depends on cell–cell junctions[5,27]. E-cadherin junctions that regulate cell–cell interactions have been identified as platforms of mechanosensing capable of transmitting forces to neighbouring cells[28–31]. The biochemical and mechanical regulations of adherens junctions through E-cadherin have been implicated during both homeostatic and oncogenic extrusions[5,16,27,32] and tumour metastasis[33]. Thus, we hypothesized that intercellular forces mediated by adherens junctions could play a role in determining the fate of extruding cells as well as their mode of extrusion, basal versus apical. In this work, we employed a comprehensive approach combining in vitro cell culture models, patient-derived xenografts and agent-based models to unveil the role of E-cadherin-based junctions in the establishment of extrusion programs. We find that the absence of E-cadherin in epithelial cells and their increased cell contractility inhibits apoptotic cell extrusion while promoting live cell invasion into the extracellular matrix when cultured on thick collagen gels or in three-dimensional (3D) gels. We use a 3D phase-field model[34] to identify the mechanical pathway that promotes various extrusion mechanisms depending on intercellular forces. In silico and experimental results reveal that cells expressing E-cadherin are subjected to higher and more persistent compressive stresses from their neighbours than cells without E-cadherin, culminating in the extrusion of live cells in monolayers without E-cadherin. We further find that live cell extrusions are associated with non-apoptotic blebbing[35] further confirmed by gene expression characterization and protein analysis. In contrast, apoptotic cells upon caspase activation display apoptotic blebbing that is followed by cell fragmentation. Our work demonstrates that different modes of cell extrusion processes are attributed to alterations in the generation, exertion and transmission of mechanical forces within the tissue leading to genetic and protein level changes.

Results

Live versus apoptotic extrusion driven by weakened cell–cell adhesions

We first used Madin–Darby canine kidney (MDCK) cells grown on fibronectin-coated plastic surfaces as a model system and investigated the impact of E-cadherin based adhesions during cell extrusion. Upon E-cadherin loss of function (hereafter referred to as E-cad KO), we observed no meaningful difference in apico-basal polarity establishment through immunostaining of ZO1 and podocalyxin (Extended Data Fig. 1a,b) and transepithelial electrical resistance measurements (TEER) (Extended Data Fig. 1c), the temporal evolution of monolayer density (Fig. 1a) or the number of extrusions (Fig. 1b) within the first 24 h. We thus focused on the first 24 h to exclude any effects from the differences in density or rate of extrusion. Here, extrusion refers to detachment of a single cell from the monolayer. Inhibition of caspase only partially inhibited extrusion events (Extended Data Fig. 2a), suggesting that some extrusions might be non-apoptotic. Surprisingly, we found a significant increase in the fraction of live cell extrusions from E-cad KO monolayers (Fig. 1c–e) through three different assays (see Supplementary Methods for details): (1) anticaspase immunostaining of fixed monolayers (Fig. 1c), (2) flow cytometry of extruded cells (Fig. 1d and Extended Data Fig. 2b) and (3) live imaging using annexin V as a reporter dye (Fig. 1e). In addition, plating the extruded cells led to colony growth of extruded cells from E-cad KO monolayers (Extended Data Fig. 2c), whereas cells extruded from wild-type (WT) monolayers did not grow upon replating. Live imaging using annexin V as an apoptosis readout confirmed a significant increase in the fraction of live extrusions within E-cad KO monolayers that constituted more than 90% of all extrusion events at early time points (Fig. 1e and Extended Data Fig. 2d,e). Here, live extrusion is defined as an event that does not express annexin V within 60 min after extrusion from the monolayer. These results were then verified by live imaging with caspase dye (Extended Data Fig. 2f)

and an endogenously tagged caspase reporter (Extended Data Fig. 2g). Moreover, rescue experiments, where E-cadherin was re-introduced, showed live extrusion profiles similar to WT monolayers (mWTs) (Fig. 1e and Extended Data Fig. 2d,e). This confirms that the outlined effects are indeed due to E-cad KO (Fig. 1e and Extended Data Fig. 2d,e). Altogether, our data reveal that E-cad KO affects the fate of extruding cells and increases the proportion of live cell extrusions.

Mechanical forces determine the fate of extruding cells

Previous work has shown that physical mechanisms based on crowding effects[6,12], mechanical instability[11,18,24,34], microtubule disassembly[36] and topological rearrangements[18] can lead to cell extrusion. Thus, we hypothesized that E-cadherin loss[37] could impact the fate of extruding cells through changes in mechanical stresses. To test this hypothesis, we first focused on mechanical stress patterns around extrusion sites using a recently developed 3D phase-field model of the cell monolayer[34] in which cell–cell and cell–substrate adhesion strengths are considered explicitly and tuned independently (see Supplementary Methods for model details and parametrization) (Extended Data Fig. 2h). Cell extrusion, in this model, is an emergent behaviour from modelling the full 3D dynamics of cell shape changes in a monolayer that affects the in-plane and out-of-plane forces acting on a cell. As such, extrusion events occur without any explicit threshold or external artificial means of favouring extrusion. Once the out-of-plane forces acting on a cell overpower the forces keeping it in the monolayer and on the substrate, a cell extrusion occurs. The main differences in mechanical imprints of WT relative to E-cad KO cells are a concomitant decrease in cell–cell adhesion, increase in cell–matrix adhesion as previously shown[37], reduced cell velocity (Extended Data Fig. 3a), increase in cell traction forces (Extended Data Fig. 3b), no change in average isotropic stress (Extended Data Fig. 3c) and an increase in cell stiffness (Extended Data Fig. 3d). Therefore, using the model, we compared the evolution of mechanical stress around extrusion sites for two different scenarios: (1) a model wild-type monolayer (mWT) with strong cell–cell contacts, weak cell–substrate interaction forces and low stiffness (Supplementary Video 1) relative to (2) a model E-cad KO monolayer (mE-cad KO) with weaker cell–cell contacts, stronger cell–substrate interaction forces and higher stiffness (Supplementary Video 2).

In silico modelling revealed a more pronounced compressive stress buildup over time near extruding mWT cells compared with mE-cad KO cells in a region of about two cell sizes (Fig. 2a). We thus computed the ensemble average of time-averaged isotropic stress fields around extrusions in our model (Fig. 2b). Interestingly, the corresponding probability density function is non-symmetric (Fig. 2c) and together with the cumulative distribution function (Fig. 2d) indicates a pronounced and persistent compressive stress buildup near extruding mWT cells, given the distribution tails and the time-averaged nature of these local fields. At the same time, the probability density corresponding to the averaged stress fields around extruding mE-cad KO cells is almost symmetric with respect to its peak, with a slight shift towards compressive (negative) stresses. Comparing the shape and the range of distributions indicates relatively high local field fluctuations near extruding mWT cells (Fig. 2c,d and Extended Data Fig. 3e). Because E-cad KO cells have a higher stiffness relative to their WT counterparts, we hypothesized that the large and persistent compressive stresses in mWT cells (Fig. 2c,d) could be due to the longer shape relaxation times (t_{shape}) for more compliant cells given by $t_{shape} \approx \gamma^{-1}$, where γ corresponds to cell stiffness in the model (see Supplementary Methods for details). Indeed, the measured shape relaxation times are longer for WT cells (Extended Data Fig. 3f) and on a similar order of magnitude as predicted by the linear stability analysis of the shape relaxation from the model (Supplementary Methods). Thus, longer shape relaxation time combined with high fluctuating stresses can lead to localization of compressive stresses, as seen for extruding mWT cells, whereas stiffer mE-cad KO cells can relax into their preferred shapes on a shorter time scale.
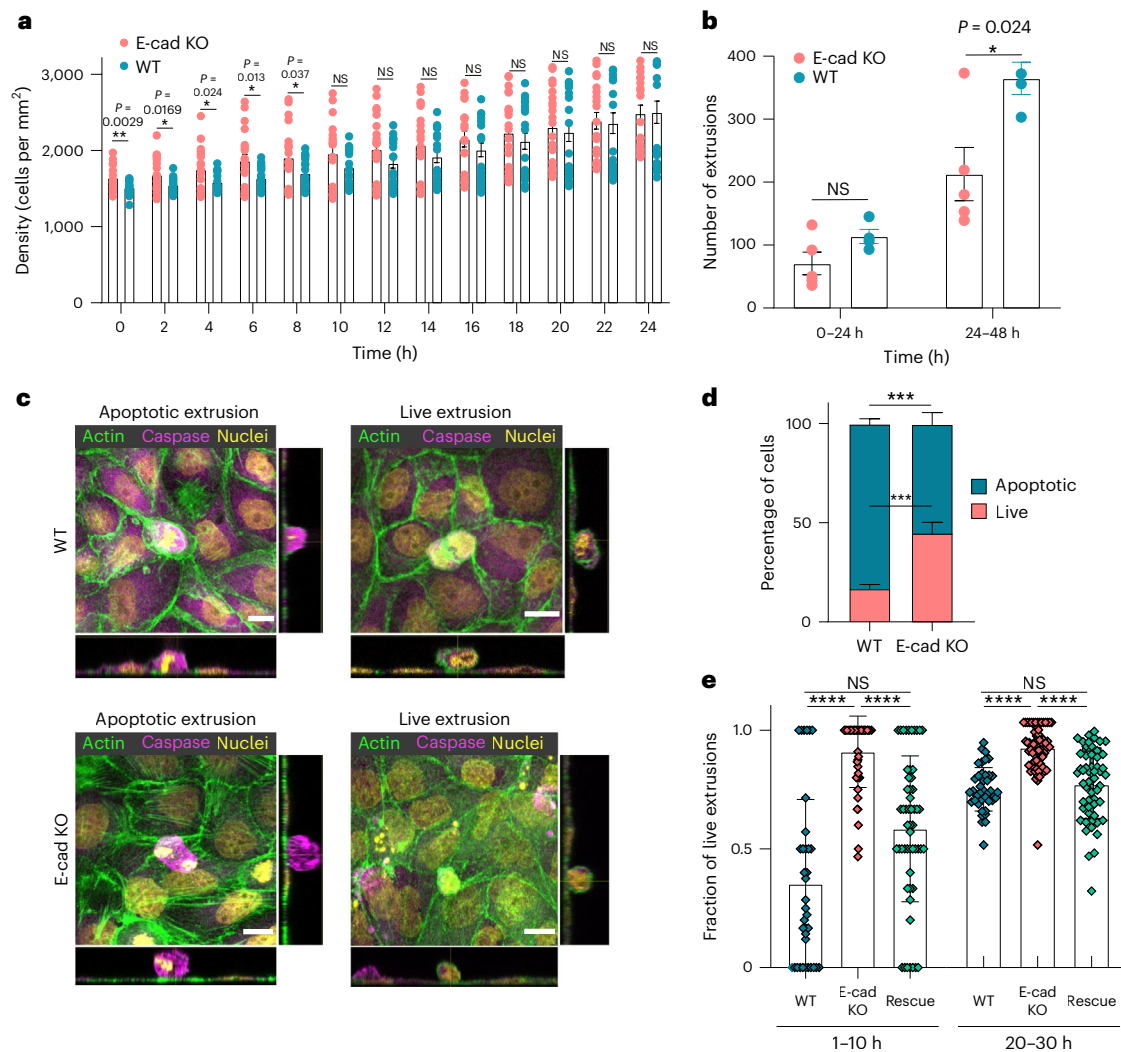
Fig. 1 | E-cad KO leads to an increase in live cell extrusion within epithelial monolayers. a, Bar plot showing the time evolution of mean density (number of cells per mm²) over an area of 0.5 mm² over the analysed time window of 0–24 hours for both WT (blue) and E-cad KO (red) monolayers. Error bars represent standard error mean (s.e.m.). *$P < 0.05$, **$P < 0.01$, and no significance (NS) represents $P > 0.05$. $n = 21$ for E-cad KO, and $n = 22$ for WT using unpaired *t*-test from two independent experiments. **b**, Bar plots showing the number of extrusions averaged over 0–24 and 24–48 hours for both WT (blue) and E-cad KO (red) monolayers. Error bars represent s.e.m. *$P < 0.05$ and NS represents $P > 0.05$); $n = 5$ for E-cad KO, and $n = 4$ for WT from an unpaired *t*-test from two independent experiments. **c**, Maximum intensity projections of immunostained MDCK WT (top) and MDCK E-cad KO (bottom) monolayers showing apoptotic (caspase positive, magenta) and live (caspase negative, magenta) cell extrusions

stained for actin (green) and nuclei (yellow). Scale bar, 50 μm. **d**, Average percentage of live cell (propidium iodide negative) and dead (propidium iodide positive) extrusions obtained through cytometry based sorting from nine different samples from two independent experiments after 24 hours of plating (100% confluency). ***$P < 0.001$ from an unpaired *t*-test. Error bars represent s.e.m. **e**, Fraction of live (annexin negative) and apoptotic (annexin positive) extrusions obtained from MDCK WT, MDCK E-cad KO, MDCK E-cad KO⁺ E-cad GFP averaged over the first 10 hours and time period 20–30 hours. Data presented are averaged over 36 (WT), 62 (E-cad KO) and 55 (E-cad KO⁺ E-cad GFP) events from two independent experiments. *P* values were obtained from Kruskal–Wallis test where ****$P < 0.0001$ and $P > 0.05$ is no significance (NS). Error bars here represent standard deviation.

To test these predictions, we turned to experimentally measured stress fields in WT and E-cad KO monolayers. We measured monolayer stress[38] and tracked how local stresses evolved in a small region of 50 μm (approximately spanning two–three cell sizes) around the cell extrusion site. The comparison of spatially averaged stress patterns around dead and live cell extrusions for both WT and E-cad KO cells revealed distinct mechanical signatures. As predicted by the model, the isotropic stress evolution with time prior to extrusion showed a threefold increase of compression in WT-apoptotic extrusions compared with E-cad KO-live extrusions in the time interval 25 min before cell extrusion (Fig. 2e), where time zero marks the time point at which the cell detached from the monolayer (Extended Data Fig. 3g,h). This peak in stress precedes caspase activation by 20–40 min in WT-apoptotic extrusions (Extended Data Fig. 3i). A similar

trend of high isotropic stress was observed for E-cad KO-apoptotic extrusion in comparison to WT-live extrusions (Extended Data Fig. 3j–l). However, it does not exclude a potential contribution from caspase at low undetectable levels[39]. Furthermore, the ensemble average of the time-averaged spatial isotropic stress fields around extrusion events revealed the dominance of compressive stresses around apoptotic extrusions in comparison to live extrusion events (Fig. 2f). Remarkably, both the probability density function (Fig. 2c) and the cumulative distribution function (Fig. 2d) associated with the local averaged experimental fields (Fig. 2f) were consistent with modelling results. Altogether, our experimental and computational observations highlight the roles of cell stiffness and stress fluctuations in localizing compressive stresses around extruding cells and consequently forging cell fate.
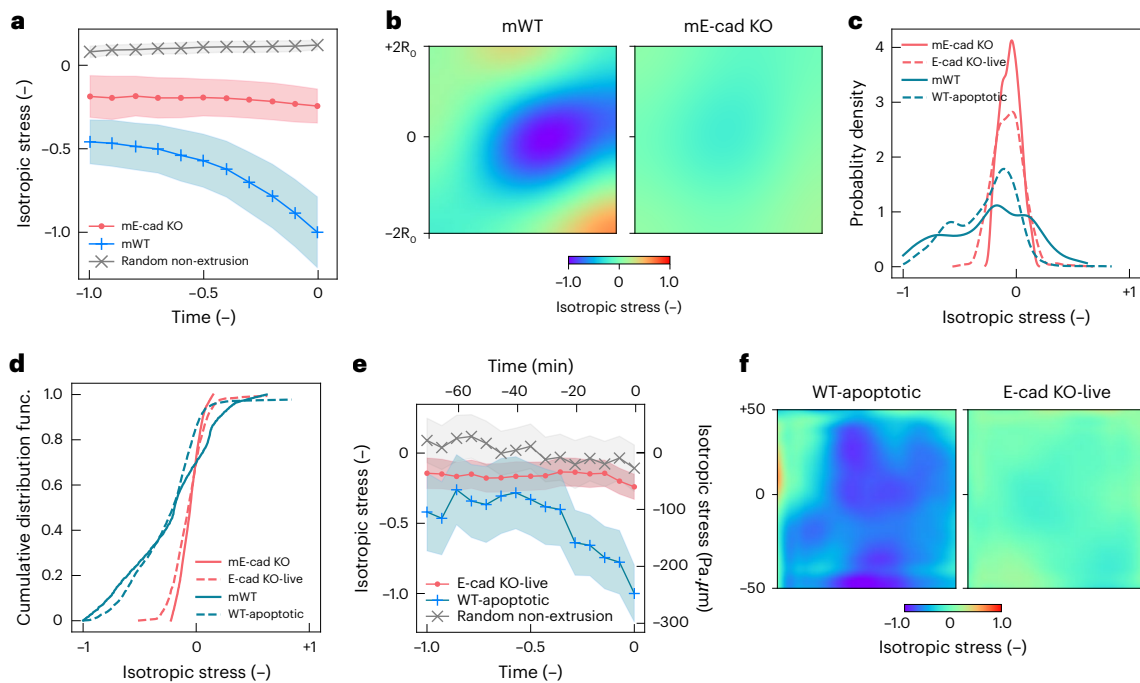
Fig. 2 | Local field statistics unravel the mechanical determinants for the fate of an extruding cell. a, Time evolution prior to an extrusion event and hence the negative sign of the spatially averaged isotropic stress, in a square domain of two cell sizes, based on 20 simulations representing 22 mE-cad KO (pink) and 21 mWT (blue) extrusion events. Also included are randomly chosen non-extrusion events ($n = 100$, grey) for the same temporal window. Error bars represent standard error. **b**, Time-averaged over the temporal window in **a** and ensemble-averaged (over n events) isotropic stress fields representing $n = 21$ extrusion events for mWT (left) and $n = 22$ extrusion events for mE-cad KO (right) obtained from 20 simulations normalized by the maximum value of compression in mE-cad KO cells. **c**, Probability density function corresponding to the averaged isotropic stress maps for simulations (mWT (solid blue), mE-cad KO (solid pink)) (**b**) and experiments (WT-apoptotic (dotted blue); E-cad KO-live (dotted pink)) (**f**). **d**, Cumulative distribution functions corresponding to probability density in **c**, clearly showing the range of the data and the persistence of compressive stresses in mWT and WT-apoptotic extruding cells. **e**, Time evolution same as

a of the spatially averaged isotropic stress in a square domain with dimensions of 50 μm × 50 μm (2–3 cell sizes) representing $n = 144$ E-cad KO-live (pink) and $n = 48$ WT-apoptotic (blue) extrusion events based on three independent experiments. Also included are random non-extrusion sites ($n = 96$, grey) for comparison. Error bars represent standard error. The second axes show the actual experimental time and stress, and the first axes (left, bottom) show the normalized time and stress. **f**, Time-averaged over the temporal window in **e** and ensemble-averaged (over n events) isotropic stress fields corresponding to $n = 37$ for WT-apoptotic (left) and $n = 109$ E-cad KO-live (right) events based on three independent experiments and normalized by the maximum compression value in E-cad KO-live cells. The temporal windows for the analyses of simulations and experiments are similar and correspond to 70 min prior to cell detachment. The mapping of the stresses in simulations and the normalization of experimental data are based on a maximum stress of −250 Pa.μm, which is compressive. The mappings between simulation units and physical ones are further detailed in the Supplementary Methods.

Cytoskeletal regulation during apoptotic and live extrusion

Next, we explored how these mechanical patterns could be linked to different signatures at subcellular levels within extruding cells. Actin cytoskeleton has been shown to be remodelled during cell extrusion[1,2,40], we thus analysed actin dynamics during both apoptotic and live cell extrusions. During apoptotic extrusions in both WT (Fig. 3a, Extended Data Fig. 4a and Supplementary Videos 3 and 4) and E-cad KO (Extended Data Fig. 4b and Supplementary Videos 5 and 6) monolayers, extruding cells undergo a reduction in basal area and aspect ratio prior to caspase activation, and we observed actin enrichment and breakage of the actin structures (Fig. 3a and Extended Data Fig. 4a), which led to apoptotic blebbing (highlighted with arrows) and eventually cell fragmentation (Fig. 3a) as previously described[35,41,42]. For live extrusions, we observed non-apoptotic blebbing of the extruding cell with actin enrichment, prior to cell rounding up and elimination from the cell monolayer for both cell types (Fig. 3b,b′, Extended Data Fig. 4c,d and Supplementary Videos 7–10) as evident from the change in basal area and aspect ratio prior to cell extrusion. In addition, we observed a higher percentage and number of live extrusions linked to non-apoptotic blebbing (Fig. 3c and Extended Data Fig. 4e). In agreement with previous measurements[37], we observed an increase in basal myosin contractility upon E-cad KO, which was validated through staining (Extended Data Fig. 5a) and western blot (Extended Data Fig. 5b,c). This increase in contractility could contribute to non-apoptotic bleb formation, as reported previously[43]. Taken

together, our results suggest that apoptotic cells subjected to high compressive stresses activate caspase, leading to cytoskeleton rupture and membrane fragmentation, whereas live extrusion favoured in E-cad KO monolayers occurs under lower compressive stresses. Currently, we cannot dismiss the potential of inherent resistance to anoikis in E-cad KO cells, which will need more exploration. However, the quantitative examination of the relationship between caspase activation and stress patterns (Extended Data Fig. 3i) suggests a probable correlation, with high compressive stresses potentially occurring before caspase activation in apoptotic extruded cells.

Upregulation of pro-survival factors

To further investigate the gene regulatory pathways associated with live cell extrusion, we conducted a comparative analysis of global-level genes and protein regulations involved in cell survival, cell death and apoptosis in MDCK WT and E-cad KO monolayers (Supplementary Methods). At both the transcriptional (Fig. 4a) and translational (Extended Data Fig. 5d) levels, we observed a reduction in cell–cell adhesion gene expression in E-cad KO cells, validating our approach. We observed an upregulation of anti-apoptotic factors, as there was a significant decrease in the expression of negatively regulating genes at the transcriptional level in E-cad KO monolayers (Fig. 4b) and translational level (Fig. 4c). Some of the upregulated proteins such as SRC[44], PTGIS[45], CD74[46] and SNCG[47] are also known to suppress apoptosis.
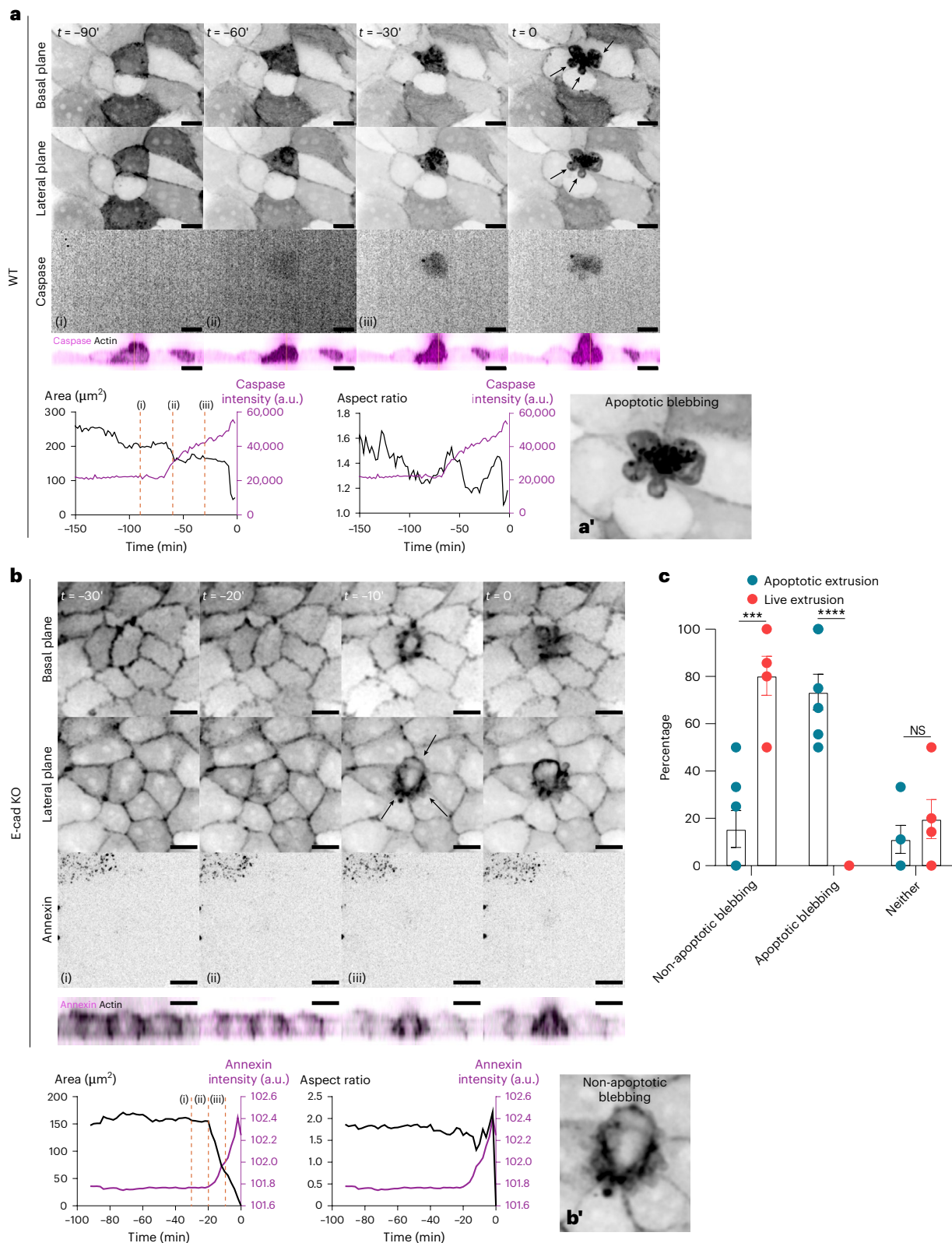
Fig. 3 | Actin dynamics regulate apoptotic versus live extrusion. a, Live imaging of LifeAct GFP (black) MDCK mWTs along with caspase dye (magenta) over time, where time shown is prior to cell extrusion, along with plots of basal area change, basal aspect ratio and caspase expression for this apoptotic extrusion event. Orange lines on the bottom-left plot indicate corresponding time points from the live imaging shown at top. **a'**, Zoomed-in version of the extruding cell marked with arrows highlighting apoptotic blebbing. **b**, Live imaging of LifeAct GFP (black) MDCK E-cad KO monolayers along with annexin dye (magenta) over time, where time shown is prior to cell extrusion, along with plots of basal area change, basal aspect ratio and annexin expression for this live extrusion event. Orange lines on the bottom-left plot indicate corresponding time points from the live imaging shown at top. **b'**, Zoomed-in version of the extruding cell, where the arrows show non-apoptotic blebbing. Scale bar, 10 μm. **c**, Averaged percentage of live or apoptotic cell extrusions that display non-apoptotic blebbing, apoptotic blebbing and neither condition. Error bars represent s.e.m. Averaged over $n = 6$ (live) and $n = 7$ (apoptotic) different experiments. ***$P < 0.001$, **$P < 0.01$, *$P < 0.05$ and NS $P > 0.05$ using t-test.
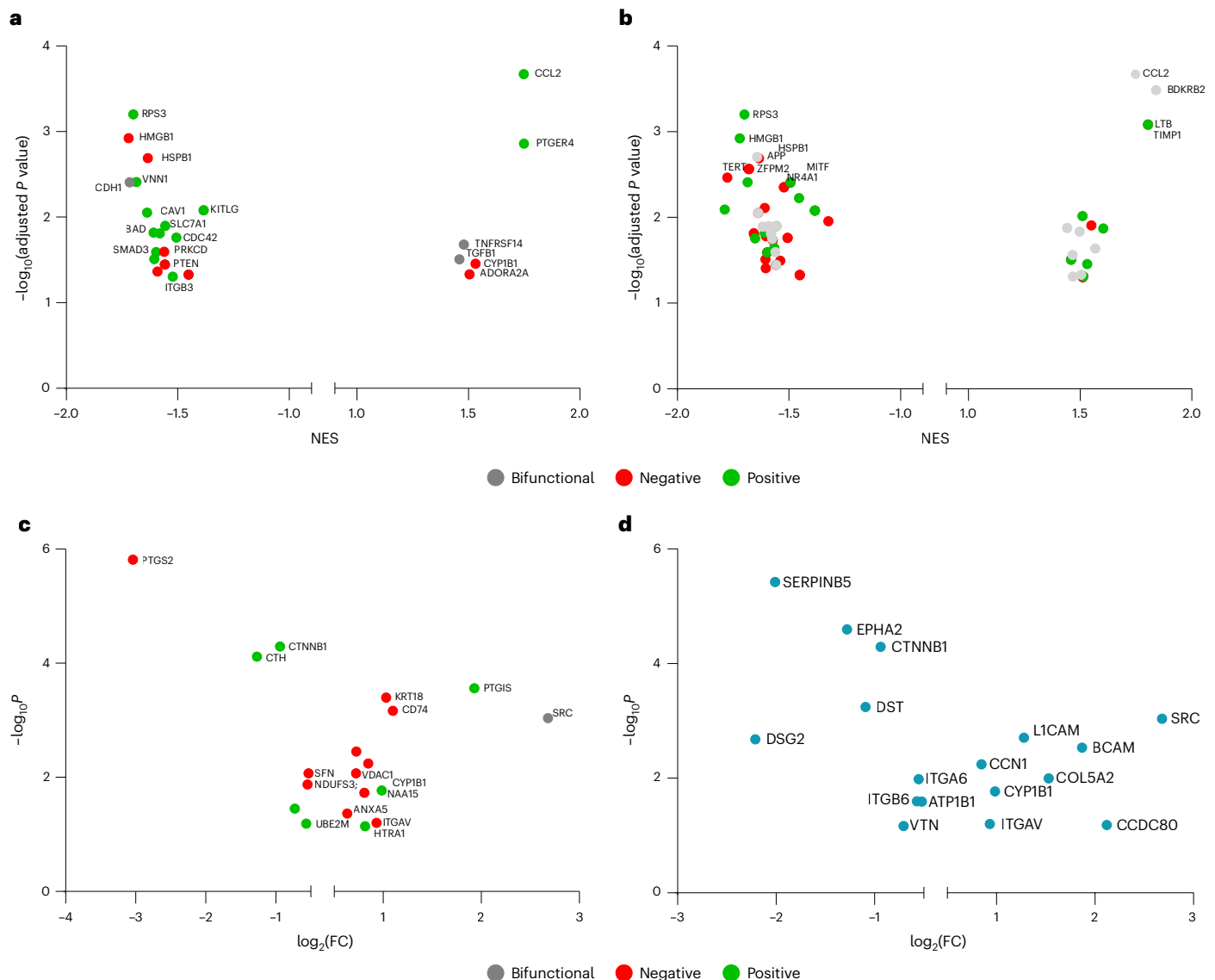
Fig. 4 | Cell death gene expression favours live cell extrusion upon E-cad KO. a, Plot of $-\log_{10}$(adjusted P value) and normalized enrichment score (NES) of cell–cell adhesion gene expression obtained from bulk sequencing. NES > 1 indicates higher expression in E-cad KO, and NES < 1 indicates lower expression in E-cad KO monolayers in comparison to mWTs. Green dots represents positive regulation, red dots negative regulation and grey dots bifunctional role of cell–cell adhesions. **b**, Plot of $-\log_{10}$(adjusted P value) and NES of genes regulating cell death obtained from bulk sequencing. Green dots represent positive regulation, red dots negative regulation and grey dots bifunctional role of cell death genes. NES > 1 indicates higher expression in E-cad KO, and NES < 1 indicates lower expression in E-cad KO monolayers in comparison to mWTs. **c**, Plot of log(fold change (FC)) and $-\log_{10} P$ of cell death regulatory protein levels obtained from proteomics. FC is the ratio of E-cad KO and WT values, meaning FC > 1 indicates higher expression in E-cad KO and FC < 1 indicates lower expression in E-cad KO in comparison to mWTs. Green represents positive regulation, red negative regulation and grey bifunctional role of cell death regulatory proteins. **d**, Plot of log(FC) and $-\log_{10} P$ of cell–matrix interaction proteins obtained from proteomics. FC is the ratio of E-cad KO and WT values, meaning FC > 1 indicates higher expression in E-cad KO and FC < 1 indicates lower expression in E-cad KO in comparison to mWTs.

Additionally, we observed a substantial regulation of actomyosin cytoskeletal proteins at the protein level, with a notable upregulation of *MYH10* (gene name for myosin IIB) (Extended Data Fig. 5e) and a phosphorylation of ML12B (protein name for MRLC) (Extended Data Fig. 5f) in E-cad KO cells, validating our earlier observation of increased contractility. This analysis provides further molecular support for the observed increase in live cell extrusion as well as for the heightened contractility (Extended Data Fig. 5a–c) of E-cad KO in comparison to WT cells, warranting further in-depth exploration in future studies.

Adherens junctions regulate apical versus basal mode of cell extrusion

We then questioned if the ability of cells to be extruded live or dead could have an impact on their mode of extrusion, basal versus apical.

Although cells are eliminated apically into the lumen during apoptotic homeostatic extrusion[48], oncogenic cell extrusion occurs via basal elimination[16,49,50]. Weakening of E-cadherin-based junctions is often associated with EMT[51] and cancer invasion[52]. Importantly, at both transcriptional (Extended Data Fig. 5g) and translational (Fig. 4d) levels, we observed significant changes in cell–matrix adhesion, with an upregulation of ITGAV (integrin), COL5A2 (collagen) and SRC (Src kinase) in E-cad KO monolayers, which could favour cell invasion. To test this in cell culture, we plated MDCK monolayers on thick two-dimensional (2D) type I collagen gels allowing basal extrusion, as stiff substrates such as glass do not allow basal extrusion. Staining for focal adhesions showed an increase in the length of focal adhesions of E-cad KO monolayers when grown on these gels (Extended Data Fig. 6a). In addition, we noticed extensive remodelling of collagen by E-cad KO monolayers (Extended
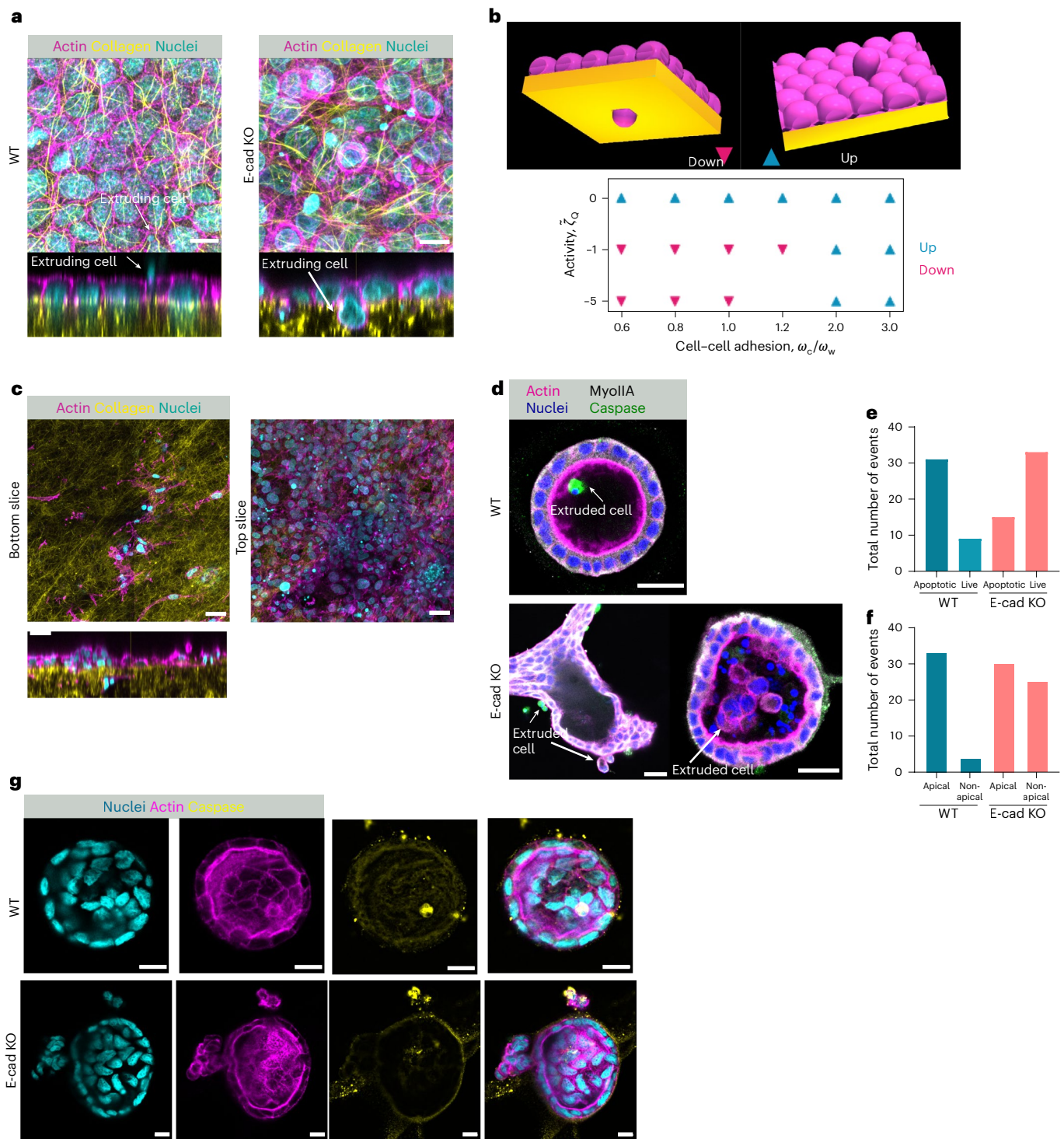
Fig. 5 | E-cad KO promotes basal cell extrusion reminiscent of tumour cell extravasation. a, Immunostaining of MDCK WT (left) and MDCK E-cad KO (right) monolayers grown on 2D type I collagen gels, actin (magenta), collagen (yellow) and nuclei (cyan). Arrows indicate extruding cells, and bottom images show the orthogonal view. Scale bars, 10 μm. **b**, Snapshots (top) and phase diagram (bottom) showing the relation between activity (contractile ($\zeta_Q < 0$), intercellular activity) and cell–cell adhesion and the direction of cell extrusions obtained from simulations demonstrating basal (down, magenta) and apical (up, blue) extrusions. Indeed, there is a finite activity threshold for basal extrusion from the model. Too small a contractility does not deform the cells. The coordinate $(\tilde{\zeta}_Q, \omega_c/\omega_w) = (-5, 1.2)$ does not go up or down. Here, $\tilde{\zeta}_Q$, ω_c and ω_w represent the strength of contractile activity, cell–cell adhesion and cell–substrate adhesion, respectively. Empty spot indicates the absence of any extrusion. **c**, Triple-negative breast cancer xenografts grown on collagen gels showing the maximum projection of few basal planes (left), apical planes (right) and the orthogonal view (bottom) immunostained for collagen (yellow), actin (magenta) and nuclei (cyan). Scale bars, 20 μm. **d**, Immunostaining of MDCK WT (top) and MDCK E-cad KO (bottom) cysts grown in matrigel for 10 days, immunostained for actin (magenta), myosin IIA (white), nuclei (blue) and caspase (green) and quantification of cysts with just apoptotic or the presence of live extrusions from $n = 40$ (WT) and $n = 48$ (E-cad KO) cysts from five independent experiments. Scale bars, 20 μm. White arrows indicate extruded cell. **e**, Distribution of extrusion events based on apoptotic or live cells for WT (blue) and E-cad KO (red). $n = 40$ (WT) and $n = 48$ (E-cad KO) cysts from five independent experiments. **f**, Distribution of extrusion events based on apical or non-apical extrusions for MDCK WT (blue) and E-cad KO (red). **g**, Immunostaining of MDCK WT (top) and MDCK E-cad KO (bottom) cysts grown in matrigel for 21 days, stained for actin (magenta), nuclei (cyan) and caspase (yellow). Scale bars, 20 μm.

Data Fig. 6a). Remarkably, both apical and basal extrusions into collagen were observed in E-cad KO monolayers, whereas all extrusions in WT monolayers remained apical (Fig. 5a and Extended Data Fig. 6b–d). Importantly, basal extrusions in E-cad KO monolayers displayed both apoptotic (annexin positive) and live (annexin negative) phenotypes (Extended Data Fig. 6b), the latter being potentially involved in cell invasion program. This observation was further confirmed by our in silico approach, where the direction of cell extrusion switched from apical to basal for a weakened cell–cell adhesion, stronger cell–substrate adhesion and enhanced contractility as observed in E-cad KO cells (Fig. 5b), capturing the competing mechanical forces that determine the mode of extrusion.

Previous studies have shown that E-cadherin levels promote single or collective cell invasion representing the early stages of the spread of cancer[51–56]. E-cadherin expression is known to be heterogeneous between different types of breast cancer cells (ductal (E-cad[+]) and intra-lobular (E-cad[−]) carcinoma)[57] and is observed in very aggressive breast metaplastic cancers[58]. This cancer is characterized by the histological presence of at least two cellular types, typically epithelial (E-cad[+]) and mesenchymal (E-cad[−]/vimentin^{+}) cells. To further probe our hypothesis of E-cad KO–driven basal extrusion, we analysed tumoroids isolated from triple-negative metaplastic patient-derived xenografts grown on 2D type I collagen gels[59]. Over time, we observed basal extrusion of E-cad^{−/−} cells with intact nuclei indicating live extrusions (Fig. 5c), further demonstrating the generality of our findings from epithelial cell lines to human-derived cancer cells. Our observation of basal extrusion of E-cad KO cells and E-cad^{−/−} breast cancer cells aligns with earlier findings associated with cancer cell invasion[53,54], which precedes the dissemination of cancer cells. Nevertheless, cancer progression is a highly intricate, pleiotropic and multifaceted process, and there are instances where E-cadherin may be necessary for cancer cell survival and metastasis[52], whereas E-cadherin loss has been associated with invasion[53–56].

We finally asked whether our key findings of enhanced live (instead of apoptotic) extrusions and promotion of basal (instead of apical) extrusions upon E-cad KO were limited to flat epithelial monolayers. To this end, we extended our experiments to 3D cysts by growing both WT and E-cad KO cells in 3D matrigel for 10 days and 21 days. After 10 days, we observed E-cad KO cysts were heterogeneous in shape, presenting both apical and basal extrusions (Fig. 5d and Extended Data Fig. 6e). Among the basally extruded cells, we observed both caspase-positive and caspase-negative cells (Fig. 5d–f and Extended Data Fig. 6e). In contrast, in WT MDCK cysts, we only found apical and apoptotic extrusions (Fig. 5d–f). After 21 days, MDCK E-cad KO cysts showed the emergence of clumps of cells accumulating on the basal side, which was never observed in MDCK WT cysts (Fig. 5g). Altogether, our experimental and in silico observations show that low cell–substrate adhesion and high cell–cell adhesion (WT) favour apical extrusions, whereas high cell–substrate adhesion, low cell–cell adhesion and high contractility (E-cad KO) favour basal extrusions.

Discussion

Understanding how the fate of extruding cells, dead or alive, is regulated in an epithelial tissue is crucial for understanding a range of diverse fundamental biological processes including tissue growth, morphogenesis and tumour progression. Our work reveals that the weakening of cell–cell adhesion mediated by the loss of E-cadherin is a key determinant shaping not only the fate of extruding cells but also the direction of extrusion, apical versus basal. These differences between WT and E-cad KO monolayers are driven by intercellular force transmission. Intercellular force transmission modulates the mechanical stress patterns in two critical ways: (1) stress field fluctuations and (2) shape relaxation times, which change as a function of cell–cell adhesion and cell stiffness. Remarkably, our 3D modelling, purely based on physical interactions with no biochemical input, predicts distinct patterns of
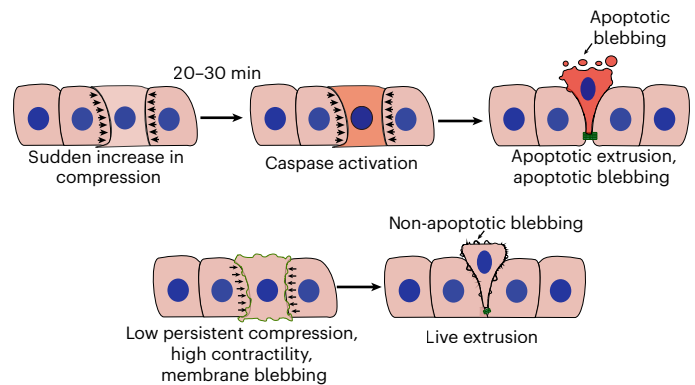

Fig. 6 | Schematic summarizing the modes of apoptotic and live extrusion within a monolayer. Top: apoptotic extrusion. Bottom: live extrusion. Apoptotic and non-apoptotic blebbing has been highlighted with arrows, and a red cell indicates caspase activation.

stress localization around extrusion sites that are corroborated in our experiments. High compressive stress in extruding WT cells, a consequence of large stress fluctuations and long shape relaxation times, correlates with caspase activation, cytoskeleton fracture and apoptotic cell fragmentation in most cases. On the other hand, an increase in contractility leads to membrane blebbing that may confer anoikis resistance and thus live cell extrusion, as summarized in Fig. 6. This observed blebbing in our experiments is in agreement with a recent study linking bleb formation in single cells to the promotion of resistance to programmed cell death (anoikis)[60] and was indicative in our gene expression analysis of cell survival pathways and cell death markers that were differentially regulated in E-cad KO cells. However, a detailed characterization to establish a causal link between blebbing and cell survival in these cell lines is a task for future research. We cannot rule out the possibility that differences in mechanical patterns could be linked to a potential higher resistance of E-cad KO cells to apoptosis. Although our study has mainly focused on the correlation between physical forces and the fate of extruding cells, exploring the combined roles of both physical and non-physical triggers in cell extrusion mechanisms is an exciting area of study for future works. The analysis of gene expression also led to the discovery of upregulated genes associated with cell–matrix adhesion, demonstrating an intriguing balance between the strength of cell–cell and cell–matrix adhesions that initiate basal extrusion. Along this line, our computational approach (Fig. 5b) showed that mE-cad KO cells with enhanced contractility, decreased cell–cell and increased cell–substrate adhesion strengths can lead to basal cell extrusions. Our experimental observations confirmed the switch from an apical extrusion mode in WT cells to apical and basal extrusions in E-cad KO cells on thick collagen gels in 2D and 3D matrices, basal extrusions often being associated with live cells in both epithelial cell lines and patient-derived xenografts.

In summary, in this work, we propose a mechanism to explain the determination of the fate of extruding cells based on the transmission of intercellular forces and cellular stiffness. Cellular extrusion mechanisms can be seen as the emergence of 3D structures from cellular monolayers and, as such, are reminiscent of morphogenetic processes[15]. The mechanism provided by our study, based on the alteration of stress patterns around the extruded cell, could therefore represent a widely applicable principle not only for understanding tissue homeostasis but also for the transition of tissues from a 2D to a 3D shape. Ultimately, our finding that stress fluctuations can trigger different modes of cell extrusion could also provide insight into epithelial multilayering in skin tissues[23], cell competition mechanisms[61] and tumour initiation[10]. Overall, we anticipate that this work will have important implications in our understanding of the regulation of tissue homeostasis and also of cell shape changes during morphogenesis[62,63] through, for instance, EMT mechanisms where E-cadherin is differently regulated as well as cancer cell invasion[64–66].

Online content

Any methods, additional references, Nature Portfolio reporting summaries, source data, extended data, supplementary information, acknowledgements, peer review information; details of author contributions and competing interests; and statements of data and code availability are available at https://doi.org/10.1038/s41567-024-02716-5.

References

1. Le, A. P. et al. Adhesion-mediated heterogeneous actin organization governs apoptotic cell extrusion. *Nat. Commun.* **12**, 397 (2021).

2. Kuipers, D. et al. Epithelial repair is a two-stage process driven first by dying cells and then by their neighbours. *J. Cell Sci.* **127**, 1229–1241 (2014).

3. Kocgozlu, L. et al. Epithelial cell packing induces distinct modes of cell extrusions. *Curr. Biol.* **26**, 2942–2950 (2016).

4. Gagliardi, P. A. et al. Mrck is activated by caspase cleavage to assemble an apical actin ring for epithelial cell extrusion. *J. Cell Biol.* **217**, 231–249 (2017).

5. Duszyc, K. et al. Mechanotransduction activates rhoa in the neighbors of apoptotic epithelial cells to engage apical extrusion. *Curr. Biol.* **31**, 1326–1336 (2021).

6. Marinari, E. et al. Live-cell delamination counterbalances epithelial growth to limit tissue overcrowding. *Nature* **484**, 542–545 (2012).

7. Eisenhoffer, G. T. & Rosenblatt, J. Bringing balance by force: live cell extrusion controls epithelial cell numbers. *Trends Cell Biol.* **23**, 185–192 (2013).

8. Roellig, D. et al. Force-generating apoptotic cells orchestrate avian neural tube bending. *Dev. Cell* **57**, 707–718.e6 (2022).

9. Monier, B. et al. Apico-basal forces exerted by apoptotic cells drive epithelium folding. *Nature* **518**, 245–248 (2015).

10. Slattum, G. M. & Rosenblatt, J. Tumour cell invasion: an emerging role for basal epithelial cell extrusion. *Nat. Rev. Cancer* **14**, 495–501 (2014).

11. Tai, K., Cockburn, K. & Greco, V. Flexibility sustains epithelial tissue homeostasis. *Curr. Opin. Cell Biol.* **60**, 84–91 (2019).

12. Eisenhoffer, G. T. et al. Crowding induces live cell extrusion to maintain homeostatic cell numbers in epithelia. *Nature* **484**, 546–549 (2012).

13. Levayer, R., Dupont, C. & Moreno, E. Tissue crowding induces caspase-dependent competition for space. *Curr. Biol.* **26**, 670–677 (2016).

14. Andrade, D. & Rosenblatt, J. Apoptotic regulation of epithelial cellular extrusion. *Apoptosis* **16**, 491–501 (2011).

15. Gracia, M. et al. Mechanical impact of epithelial-mesenchymal transition on epithelial morphogenesis in Drosophila. *Nat. Commun.* **10**, 2951 (2019).

16. Wu, S. K., Lagendijk, A. K., Hogan, B. M., Gomez, G. A. & Yap, A. S. Active contractility at e-cadherin junctions and its implications for cell extrusion in cancer. *Cell Cycle* **14**, 315–322 (2015).

17. Ranft, J. et al. Fluidization of tissues by cell division and apoptosis. *Proc. Natl Acad. Sci. USA* **107**, 20863–20868 (2010).

18. Saw, T. B. et al. Topological defects in epithelia govern cell death and extrusion. *Nature* **544**, 212–216 (2017).

19. Teo, J. L. et al. Caveolae control contractile tension for epithelia to eliminate tumor cells. *Dev. Cell* **54**, 75–91.e7 (2020).

20. Kawaue, T. et al. Inhomogeneous mechanotransduction defines the spatial pattern of apoptosis-induced compensatory proliferation. *Dev. Cell* **58**, 267–277.e5 (2023).

21. Gudipaty, S. A. et al. Mechanical stretch triggers rapid epithelial cell division through Piezo1. *Nature* **543**, 118–121 (2017).

22. Krndija, D. et al. Active cell migration is critical for steady-state epithelial turnover in the gut. *Science* **365**, 705–710 (2019).

23. Wickström, S. A. & Niessen, C. M. Cell adhesion and mechanics as drivers of tissue organization and differentiation: local cues for large scale organization. *Curr. Opin. Cell Biol.* **54**, 89–97 (2018).

24. Okuda, S. & Fujimoto, K. A mechanical instability in planar epithelial monolayers leads to cell extrusion. *Biophys. J.* **118**, 2549–2560 (2020).

25. Gagliardi, P. A. et al. Collective erk/akt activity waves orchestrate epithelial homeostasis by driving apoptosis-induced survival. *Dev. Cell* **56**, 1712–1726.e6 (2021).

26. Valon, L. et al. Robustness of epithelial sealing is an emerging property of local erk feedback driven by cell elimination. *Dev. Cell* **56**, 1700–1711.e8 (2021).

27. Lubkov, V. & Bar-Sagi, D. E-cadherin mediated cell coupling is required for apoptotic cell extrusion. *Curr. Biol.* **24**, 868–874 (2014).

28. le Duc, Q. et al. Vinculin potentiates E-cadherin mechanosensing and is recruited to actin-anchored sites within adherens junctions in a myosin ii-dependent manner. *J. Cell Biol.* **189**, 1107–1115 (2010).

29. Borghi, N. et al. E-cadherin is under constitutive actomyosin-generated tension that is increased at cell-cell contacts upon externally applied stretch. *Proc. Natl Acad. Sci. USA* **109**, 12568–12573 (2012).

30. Bazellières, E. et al. Control of cell–cell forces and collective cell dynamics by the intercellular adhesome. *Nat. Cell Biol.* **17**, 409–420 (2015).

31. Kale, G. R. et al. Distinct contributions of tensile and shear stress on E-cadherin levels during morphogenesis. *Nat. Commun.* **9**, 5021 (2018).

32. Schipper, K. et al. Rebalancing of actomyosin contractility enables mammary tumor formation upon loss of E-cadherin. *Nat. Commun.* **10**, 3800 (2019).

33. Na, T.-Y., Schecterson, L., Mendonsa, A. M. & Gumbiner, B. M. The functional activity of E-cadherin controls tumor cell metastasis at multiple steps. *Proc. Natl Acad. Sci. USA* **117**, 5931–5937 (2020).

34. Monfared, S., Ravichandran, G., Andrade, J. & Doostmohammadi, A. Mechanical basis and topological routes to cell elimination. *eLife* **12**, e82435 (2023).

35. Bovellan, M., Fritzsche, M., Stevens, C. & Charras, G. Death-associated protein kinase (dapk) and signal transduction: blebbing in programmed cell death. *FEBS J.* **277**, 58–65 (2010).

36. Villars, A., Matamoro-Vidal, A., Levillayer, F. & Levayer, R. Microtubule disassembly by caspases is an important rate-limiting step of cell extrusion. *Nat. Commun.* **13**, 3632 (2022).

37. Balasubramaniam, L. et al. Investigating the nature of active forces in tissues reveals how contractile cells can form extensile monolayers. *Nat. Mater.* **20**, 1156–1166 (2021).

38. Nier, V. et al. Inference of internal stress in a cell monolayer. *Biophys. J.* **110**, 1625–1635 (2016).

39. Nano, M., Mondo, J. A., Harwood, J., Balasanyan, V. & Montell, D. J. Cell survival following direct executioner-caspase activation. *Proc. Natl Acad. Sci. USA* https://doi.org/10.1073/pnas.2216531120 (2023).

40. Rosenblatt, J., Raff, M. C. & Cramer, L. P. An epithelial cell destined for apoptosis signals its neighbors to extrude it by an actin- and myosin-dependent mechanism. *Curr. Biol.* **11**, 1847–1857 (2001).

41. Aoki, K. et al. Coordinated changes in cell membrane and cytoplasm during maturation of apoptotic bleb. *Mol. Biol. Cell* **31**, 833–844 (2020).

42. Walker, N. I., Harmon, B. V., Gobé, G. C. & Kerr, J. F. Patterns of cell death. *Methods Achiev. Exp. Pathol.* **13**, 18–54 (1988).

43. Goudarzi, M. et al. Identification and regulation of a molecular module for bleb-based cell motility. *Dev. Cell* **23**, 210–218 (2012).

44. Anerillas, C. et al. Early src activation skews cell fate from apoptosis to senescence. *Sci. Adv.* **8**, eabm0756 (2022).

45. Ding, H., Wang, K.-y, Chen, S.-y, Guo, K.-W. & Qiu, W.-h. Validating the role of ptgis gene in colorectal cancer by bioinformatics analysis and in vitro experiments. *Sci. Rep.* **13**, 16496 (2023).

46. Ha, S. et al. Knockdown of cd-74 in the proliferative and apoptotic activity of breastcancer cells. *Open Access Maced. J. Med. Sci.* **7**, 3169–3176 (2019).

47. Tian, L., Zhao, Y., Truong, M.-J., Lagadec, C. & Bourette, R. P. Synuclein gamma expression enhances radiation resistance of breast cancer cells. *Oncotarget* **9**, 27435–27447 (2018).

48. Gu, Y., Forostyan, T., Sabbadini, R. & Rosenblatt, J. Epithelial cell extrusion requires the sphingosine-1-phosphate receptor 2 pathway. *J. Cell Biol.* **193**, 667–676 (2011).

49. Hogan, C. et al. Characterization of the interface between normal and transformed epithelial cells. *Nat. Cell Biol.* **11**, 460–467 (2009).

50. Slattum, G., Gu, Y., Sabbadini, R. & Rosenblatt, J. Autophagy in oncogenic k-ras promotes basal extrusion of epithelial cells by degrading s1p. *Curr. Biol.* **24**, 19–28 (2014).

51. Wheelock, M. J., Shintani, Y., Maeda, M., Fukumoto, Y. & Johnson, K. R. Cadherin switching. *J. Cell Sci.* **121**, 727–735 (2008).

52. Padmanaban, V. et al. E-cadherin is required for metastasis in multiple models of breast cancer. *Nature* **573**, 439–444 (2019).

53. Ilina, O. et al. Cell-cell adhesion and 3D matrix confinement determine jamming transitions in breast cancer invasion. *Nat. Cell Biol.* **22**, 1103–1115 (2020).

54. Derksen, P. W. B. et al. Somatic inactivation of E-cadherin and p53 in mice leads to metastatic lobular mammary carcinoma through induction of anoikis resistance and angiogenesis. *Cancer Cell* **10**, 437–449 (2006).

55. Bruner, H. C. & Derksen, P. W. B. Loss of E-cadherin-dependent cell-cell adhesion and the development and progression of cancer. *Cold Spring Harb. Perspect. Biol.* **10**, a029330 (2018).

56. Melo, S. et al. The ecm and tissue architecture are major determinants of early invasion mediated by E-cadherin dysfunction. *Commun. Biol.* **6**, 1132 (2023).

57. Khalil, A. A. et al. Collective invasion in ductal and lobular breast cancer associates with distant metastasis. *Clin. Exp. Metastasis* **34**, 421–429 (2017).

58. Reddy, T. P. et al. A comprehensive overview of metaplastic breast cancer: clinical features and molecular aberrations. *Breast Cancer Res.* **22**, 121 (2020).

59. Coussy, F. et al. A large collection of integrated genomically characterized patient-derived xenografts highlighting the heterogeneity of triple-negative breast cancer. *Int. J. Cancer* **145**, 1902–1912 (2019).

60. Weems, A. D. et al. Blebs promote cell survival by assembling oncogenic signalling hubs. *Nature* **615**, 517–525 (2023).

61. Matamoro-Vidal, A. & Levayer, R. Multiple influences of mechanical forces on cell competition. *Curr. Biol.* **29**, R762–R774 (2019).

62. Guillamat, P., Blanch-Mercader, C., Pernollet, G., Kruse, K. & Roux, A. Integer topological defects organize stresses driving tissue morphogenesis. *Nat. Mat.* **21**, 588–597 (2022).

63. Engler, A. J., Sen, S., Sweeney, H. L. & Discher, D. E. Matrix elasticity directs stem cell lineage specification. *Cell* **126**, 677–689 (2006).

64. Kang, Y. & Massagué, J. Epithelial-mesenchymal transitions: twist in development and metastasis. *Cell* **118**, 277–279 (2004).

65. Antony, J., Thiery, J. P. & Huang, R. Y.-J. Epithelial-to-mesenchymal transition: lessons from development, insights into cancer and the potential of emt-subtype based therapeutic intervention. *Phys. Biol.* **16**, 041004 (2019).

66. Rübsam, M. et al. E-cadherin integrates mechanotransduction and egfr signaling to control junctional tissue polarization and tight junction positioning. *Nat. Commun.* **8**, 1250 (2017).

Reporting summary

Further information on research design is available in the Nature Portfolio Reporting Summary linked to this article.

Data availability

Sequencing dataset (GSE234079) is publicly available. Proteomics dataset is also publicly available via PRIDE (PXD043091 and PXD043091). Source data are provided with this paper.

Code availability

The code is available on GitHub: https://github.com/siavashmonfared/celadro_three_dimensional.

Author contributions

R.-M.M., A.D. and B.L. supervised the project. L.B. performed the majority of the experiments and all the experimental analysis in this paper. S.M. performed the phase-field simulations with varying adhesion strengths and stiffness. A.A. performed the phase-field simulations for apical and basal extrusions. A.S. performed the 2D collagen bed experiments and some quantification on live cell fractions with help in RNA extraction. C.R. performed the tumour xenograft experiments and some immunostaining with inputs from P.C. E.M. generated and provided human patient-derived xenograft samples. C.R. also helped with protein and RNA extraction for proteomics and sequencing. T.D. helped with protein and RNA extraction for proteomics and sequencing experiments and helped with immunostaining and western blots repeats. C.M. performed the sequencing analysis. L.K. performed the experiments in Extended Data Fig. 4a. S.D. performed part of the experiments for Extended Data Fig. 1a. R.C. performed transepithelial electrical resistance measurements. B.L.D. performed AFM measurements of WT and E-cad KO monolayers. M.H. performed nano indentation experiments to get shape relaxation times. L.B., S.M., R.-M.M., A.D. and B.L. conceived the project and wrote the paper with inputs from the other authors.

Competing interests

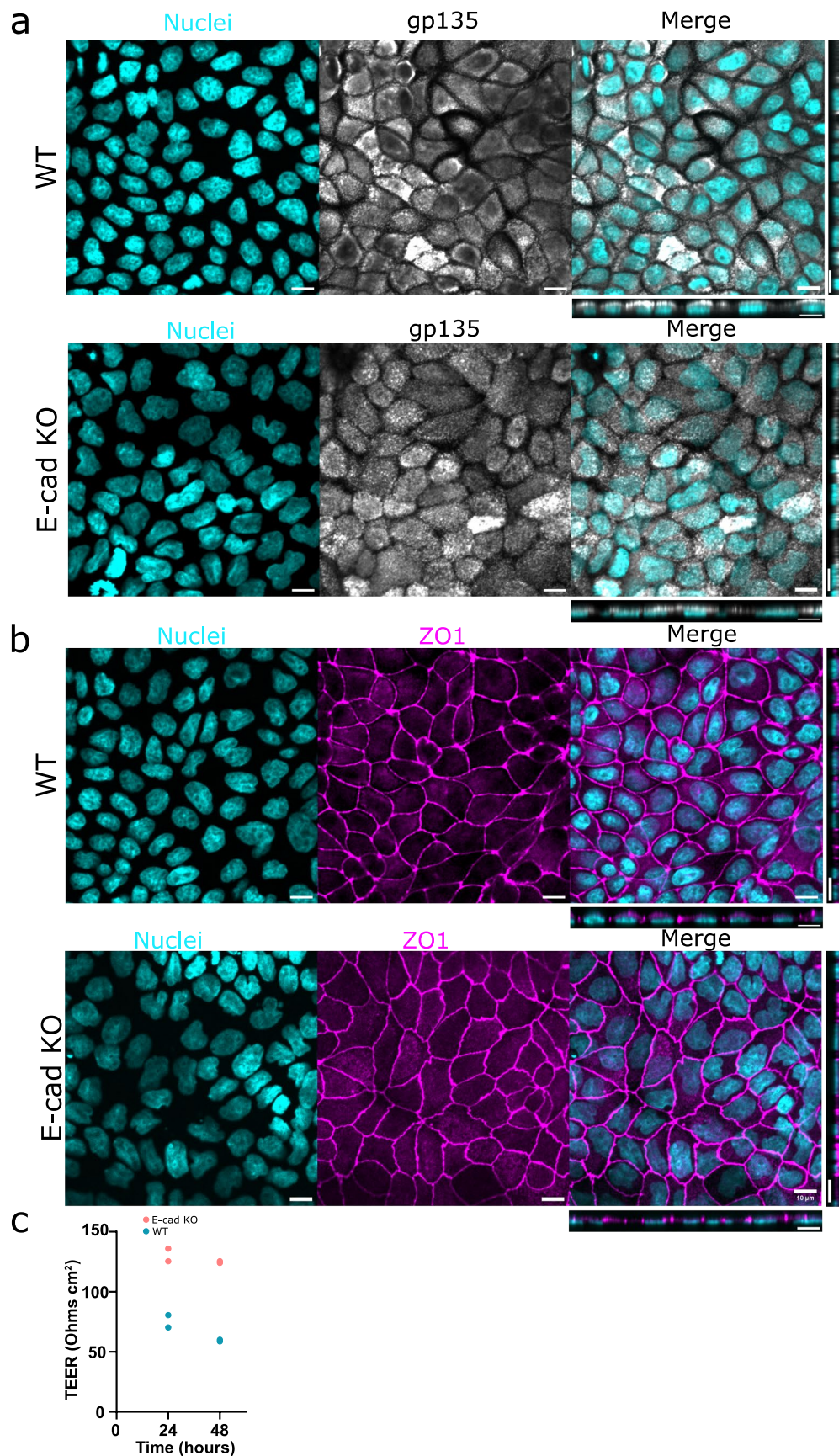The authors declare no competing interests.

Additional information

Extended data is available for this paper at https://doi.org/10.1038/s41567-024-02716-5.

Supplementary information The online version contains supplementary material available at https://doi.org/10.1038/s41567-024-02716-5.

Correspondence and requests for materials should be addressed to René-Marc Mége, Amin Doostmohammadi or Benoit Ladoux.

Peer review information *Nature Physics* thanks David Gonzalez-Rodriguez, Yuan Lin and the other, anonymous, reviewer(s) for their contribution to the peer review of this work.
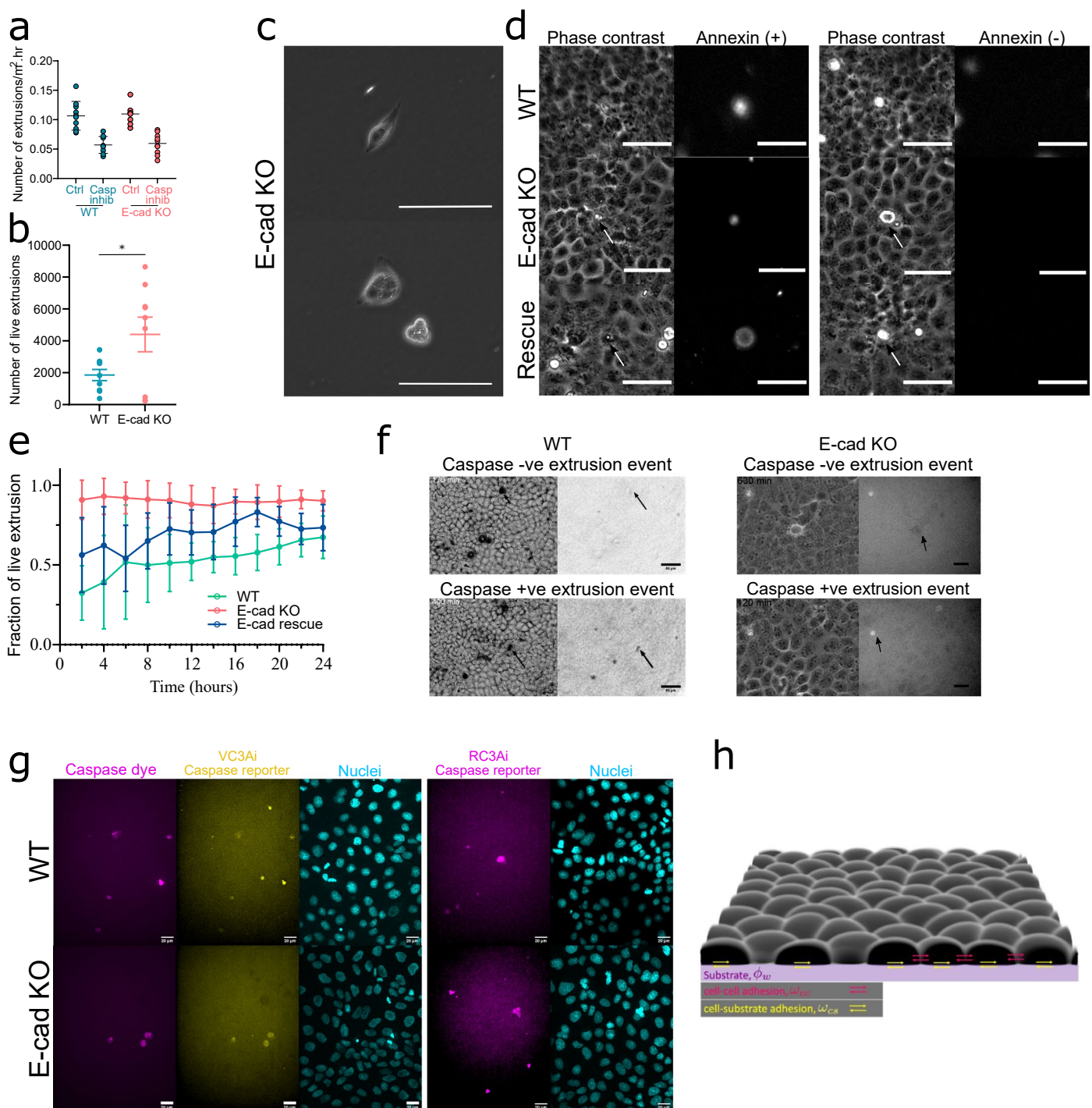
Reprints and permissions information is available at www.nature.com/reprints.

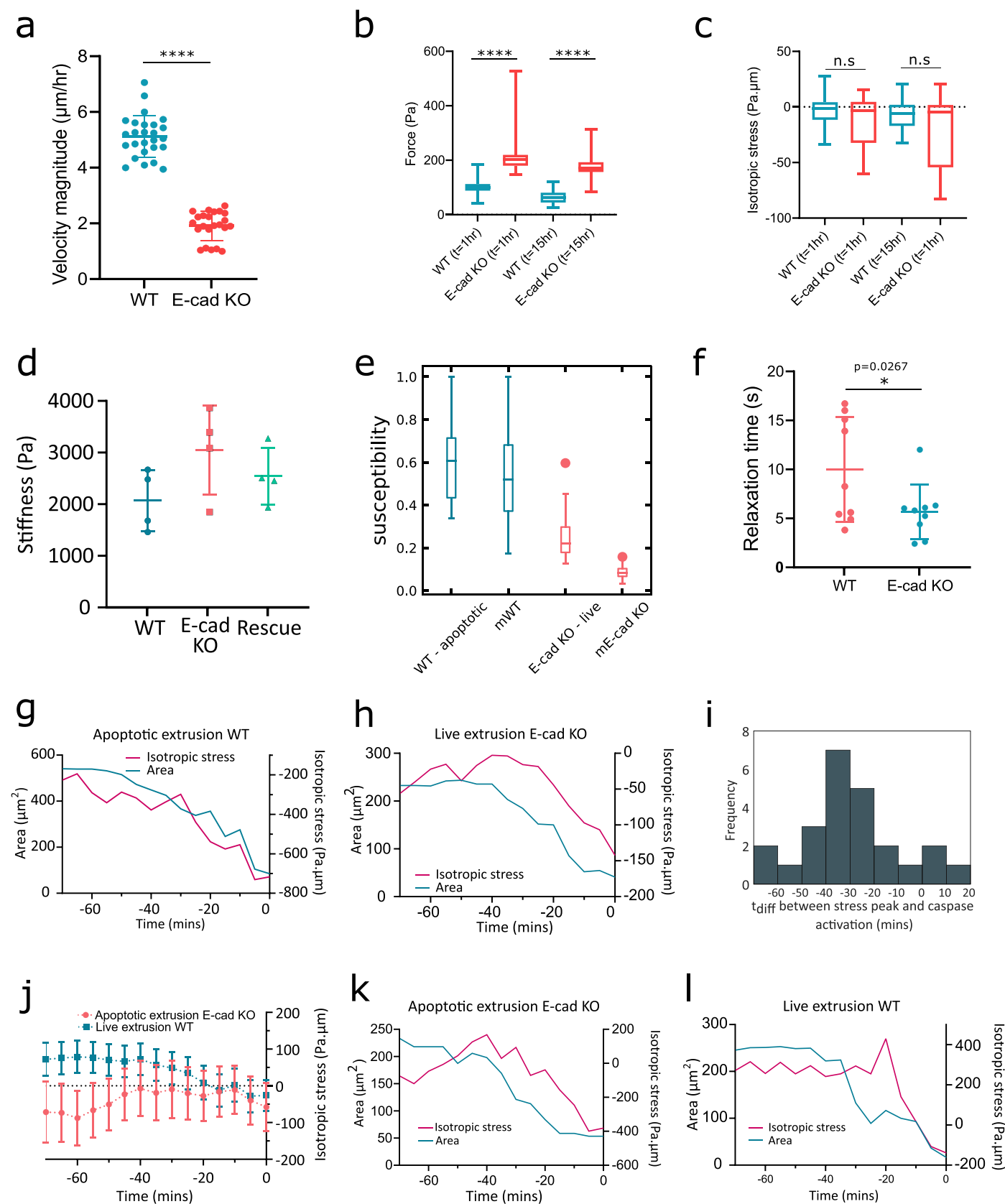**Extended Data Fig. 1 | See next page for caption.**

Extended Data Fig. 1 | Junctional integrity is maintained upon adhesion removal. Immunostaining of WT (top) and E-cad KO (bottom) monolayers for **a**) gp135 (grey) (podocalyxin) an apical marker and nuclei (cyan) showing the orthogonal view. **b**) ZO1 a tight junction marker (magenta) and nuclei (cyan) along with their orthogonal view, showing that both WT (top) and E-cad KO (bottom) monolayers are polarized at the stages analyzed in this manuscript. Scale: 10μm. **c**) TEER values from 2 different samples grown on transwell filters 24 and 48 hours after confluency representative of the densities presented in this work for both WT (blue) and E-cad KO (red) monolayers.

Extended Data Fig. 2 | E-cadherin removal results in an increase in live cell extrusion. a) Number of extrusions per mm² per hr for both MDCK WT (blue) and MDCK E-cad KO (pink) monolayers that are treated with caspase inhibitor Z-VAD FMK and the control untreated samples (n=10, WT control, n=9 wt caspase inhibition, n=7 E-cad KO control, n=10 E-cad KO caspase inhibition) from 2 independent experiments. **b)** Average of absolute number of live extrusions for both MDCK WT (blue) and MDCK E-cad KO (pink) obtained from cytometry where the error bar represents the SEM from 9 samples from 2 independent experiments. p value = 0.038 obtained from Kolmogorov-Smirnov test. **c)** Examples of extruded E-cad KO cells from confluent monolayers that were replated and grew. Scale: 100μm. **d)** Snapshots obtained from a time lapse image of MDCK WT (top), E-cad KO (middle) and E-cad KO rescue (bottom) showing cell extrusion that are annexin V labelled (apoptotic, left) and annexin V negative

(live, right). Arrows indicate the extruded cell. Scale: 50μm. **e)** Fraction of live extrusions over time obtained from live imaging of MDCK WT (n=11, green), E-cad KO (n=13, pink) and E-cad KO with E- cadherin rescue (n=12, blue). **f)** Snapshots of MDCK WT and MDCK E-cad KO monolayers, stained with caspase dye (right) along with the phase contrast image (left) showing the site of extrusion. Arrows indicate the extruded cell. Caspase positive extrusions are labelled as +ve and caspase negative extrusions are labelled as -ve. Scale: 50μm. **g)** Live imaging of MDCK WT (top) and MDCK E-cad KO (bottom) monolayers that are endogenously tagged with a caspase reports (VC3Ai/ RC3Ai) and co-stained with caspase dye. These monolayers were stained for nuclei with Hoescht (cyan) during live imaging. Scale: 20μm. h) An example cross-section from a simulation. The arrows show, schematically, how cell-cell and cell-substrate adhesions are explicitly accounted for in our modeling approach and mathematically outlined in the Methods.
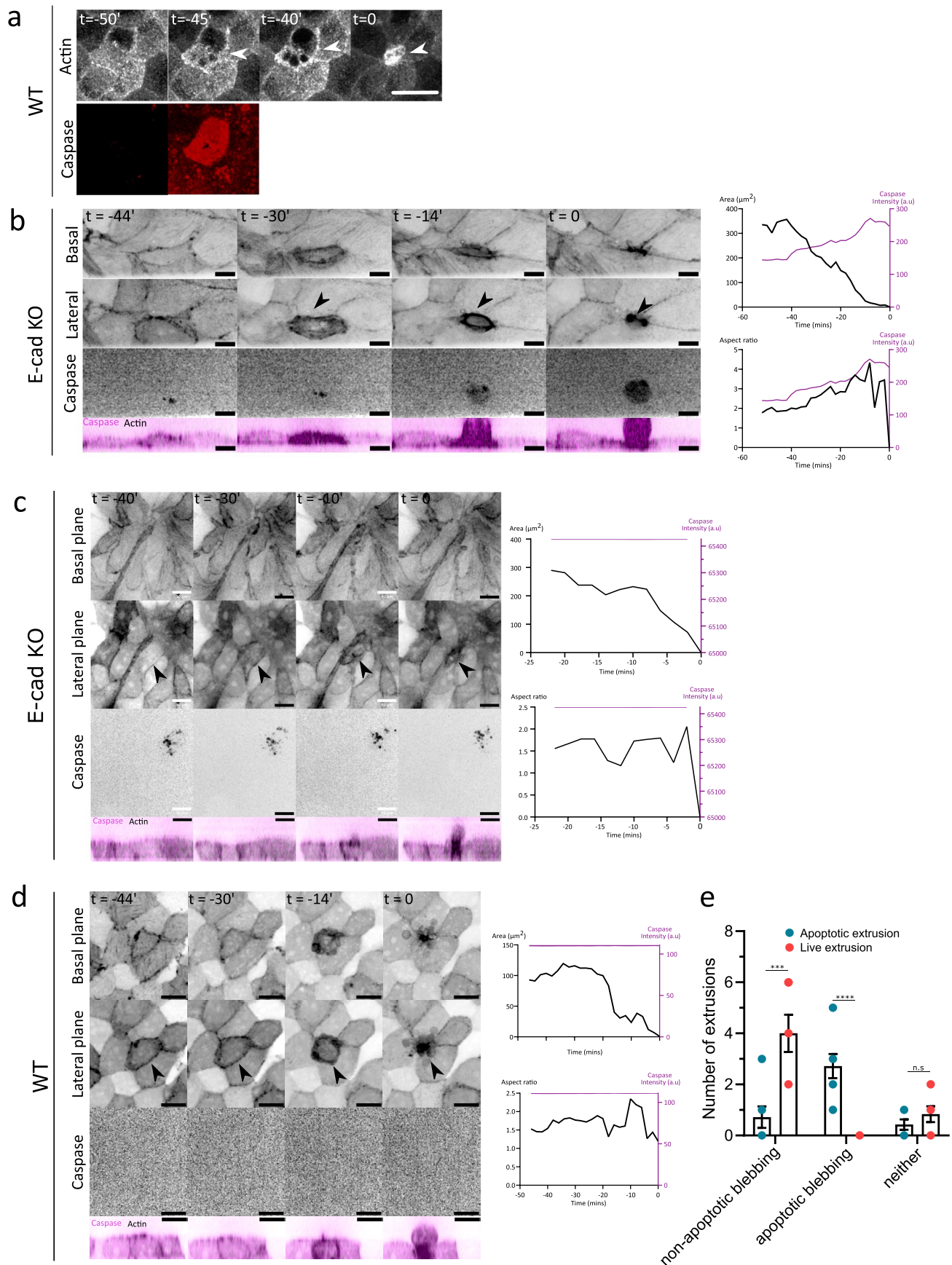
Extended Data Fig. 3 | See next page for caption.

Extended Data Fig. 3 | Stress changes determine the fate of extruded cells.
a) Scatter plot of velocity magnitude averaged over a 10 hours time period for both WT (blue) and E-cad KO monolayers (red). Error bars represent standard deviation (SD) for velocity where n =26 for WT and n= 23 for E-cad KO from 2 independent experiments. **b**) Box plot traction force magnitudes averaged over the 1st hour of imaging and the 15th hour of imaging for both WT (blue) and E-cad KO (red) monolayers. n= 30 for WT and n= 16 for E-cad KO from 2 independent experiments for traction force. **c**) Box plots of averaged monolayer isotropic stress averaged over the 1st hour of imaging and 15th hour of imaging for both WT (blue) and E-cad KO (red) monolayers. For stress, n =46 for WT and n= 29 for E-cad KO from 2 independent experiments. Here no significance (n.s.) refers to p > 0.05 and **** represents p < 0.0001 from two-tailed unpaired t-test for velocity and two-tailed Kolomogrov Smirnov test (stress and force). Whiskers in **b**) and **c**) represent the min and max values of the dataset. **d**) Mean stiffness of cells within a monolayer obtained via AFM from 4 different samples for each condition. Error bars represent standard deviation (SD). **e**) The susceptibility of the local isotropic stress fields near extruding cells at and prior to the extrusions showing higher field fluctuations for mWT (in-silico) and WT - apoptotic (experiments) cases relative to mE-cad KO (in-silico) and E-cad KO - live (experiments). The values are normalized by the maximum for mWT and WT - apoptotic cases. The temporal

window for the analyses of simulations and experiments are similar (Methods). Furthermore, simulation time and computed stress are non-dimensionalized (Methods). The whiskers here represent the min and max values. **f**) Mean relaxation time of confluent WT and E-cad KO cells obtained from n=9 (WT and E-cad KO) samples from a single experiment. * represents p < 0.05 through a one-tailed Welch's t-test. Error bars represent standard deviation. **g**, **h**) Representative example of the evolution of spatially averaged isotropic stress over a region of 50x50μm (pink) and basal area (blue) over time where time zero is point at which basal area becomes zero for **g**) apoptotic extrusion (WT) and **h**) live extrusion in an E-cad KO monolayer. **i**) Histogram showing the time difference between increase in stress and caspase activation during WT apoptotic extrusions from n= 24 events from 2 independent experiments. **j**) Time evolution of averaged isotropic stress around a square region of 50x50μm around the extruding cell prior to extrusion averaged over 26 (E-cad KO apoptotic) and 96 (WT live) extrusions from 3 independent experiments. Error bars represent standard error. **k**, **l**) Representative example of the evolution of spatially averaged isotropic stress over a region of 50x50μm (pink) and basal area (blue) over time where time zero is point at which basal area becomes zero for **k**) apoptotic extrusion (E-cad KO) and **l**) live extrusion in a WT monolayer.
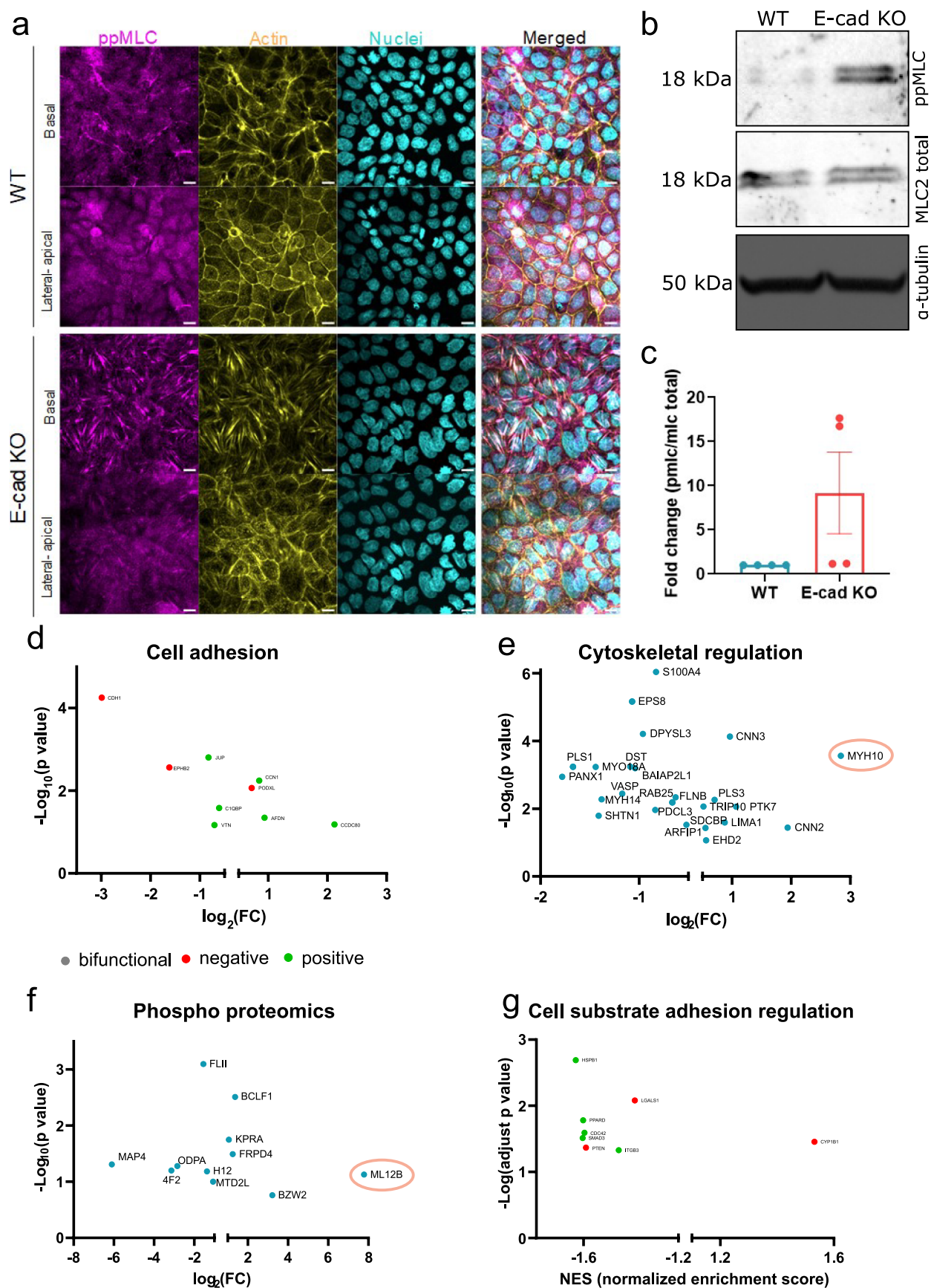
Extended Data Fig. 4 | See next page for caption.

Extended Data Fig. 4 | Cytoskeletal changes underlie apoptotic vs live extrusion. a) Confocal images in the midplane from a time lapsed sequence of the apoptotic cell extrusion labeled with actin-GFP (grey), and Caspase-3 (red). At t = 0 the apoptotic cell is eliminated from the monolayer. The emergence of cavities inside the cytosolic F-actin is observed in this example. Scale: 10μm. **b**) Time lapse example of apoptotic extrusion of lifeact GFP (grey) labeled MDCK E-cad KO monolayers at the basal (top), mid-lateral (middle)and apical (bottom) planes obtained through spinning disk confocal imaging, stained with caspase (magenta) dye, where time t=0 indicates the time point at which basal area is zero. Side view showing extrusion across time. Time is in minutes and indicated with ′ symbol. Quantifications show the evolution of basal area, aspect ratio against caspase intensity over time where time zero is time at which basal area is zero and time prior defined as -t mins. Scale: 10μm. **c**) Time lapse example of live extrusion of lifeact GFP (grey) labeled MDCK E-cad KO monolayers at the basal (top), mid-lateral (middle)and apical (bottom) planes obtained through spinning disk confocal imaging, stained with caspase (magenta) dye, where time t=0
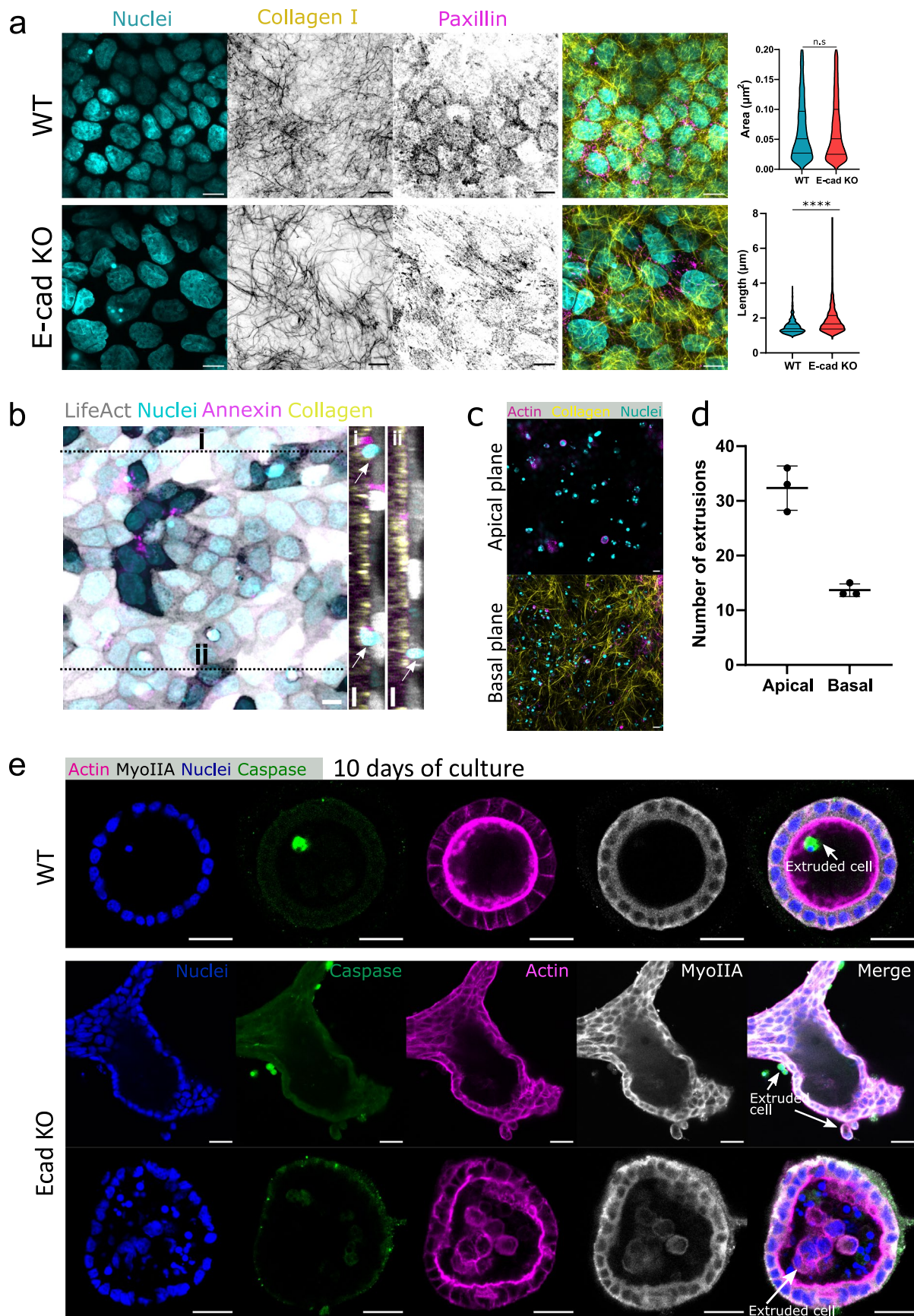
indicates the time point at which basal area is zero. Side view showing extrusion across time. Time is in minutes and indicated with ′ symbol. Quantifications show the evolution of basal area, aspect ratio against caspase intensity over time where time zero is time at which basal area is zero and time prior defined as -t mins. **d**) Time lapse example of live extrusion of lifeact GFP (grey) labeled MDCK WT monolayers at the basal (top), mid-lateral (middle)and apical (bottom) planes obtained through spinning disk confocal imaging, stained with caspase (magenta) dye, where time t=0 indicates the time point at which basal area is zero. Side view showing extrusion across time. Time is in minutes and indicated with ′ symbol. Quantifications show the evolution of basal area, aspect ratio against caspase intensity over time where time zero is time at which basal area is zero and time prior defined as -t mins. Scale: 10μm. **e**) Total number of live or apoptotic cell extrusions that display non-apoptotic blebbing, apoptotic blebbing and neither condition. Error bars represent SEM. Averaged over n=6 (live) and n =7 (apoptotic) different experiments. *** $p < 0.001$, ** $p < 0.01$, * $p < 0.05$ and n.s indicates non-significant ($p > 0.05$) using unpaired t-test.

Extended Data Fig. 5 | See next page for caption.

Extended Data Fig. 5 | Cytoskeletal changes trigger live cell extrusion upon E-cadherin loss of function. a) Immunostaining of ppMLC (T18/S19) (magenta), actin (yellow) and nuclei (cyan) of WT (top) and E-cad KO (bottom) monolayers highlighting both apical and basolateral regions. Scale: 10μm. **b**) Western blot of WT and E-cad KO monolayers for ppMLC and MLC total and the **c**) fold change of phosphorylation quantified as the ratio of ppMLC/ MLC total obtained from 4 different samples. Error bars represent S.D. **d**) Plot of log (fold change) and -log (p value) of cell adhesion proteins obtained from proteomics. Fold change (FC) is the ratio of E-cad KO/ WT values, meaning FC > indicates higher expression in E-cad KO (in pink) and FC < 1 indicates lower expression in E-cad KO (in blue) in comparison to WT monolayers. **e**) Plot of log (fold change) and -log (p value) of cytoskeletal proteins obtained from proteomics. Fold change (FC) is the ratio of E-cad KO/ WT values, meaning FC > indicates higher expression in E-cad KO and

FC < 1 indicates lower expression in E-cad KO in comparison to WT monolayers. Circled gene is MYH10 a known contractility regulator. **f**) Plot of log (fold change) and -log (p value) of the proteins obtained from proteomics that were phosphorylated. Fold change (FC) is the ratio of E-cad KO/ WT values, meaning FC > indicates higher expression in E-cad KO and FC < 1 indicates lower expression in E-cad KO in comparison to WT monolayers. Circled gene is ML12B a known contractility regulator. **g**) Plot of -log(p value) and normalized enrichment score (NES) of cell-substrate adhesion gene expression obtained from bulk sequencing. NES > 1 indicates higher expression in E-cad KO and NES < 1 indicates lower expression in E-cad KO monolayers in comparison to WT monolayers. Green represents positive regulation, red negative regulation and grey bifunctional role of cell death regulation.
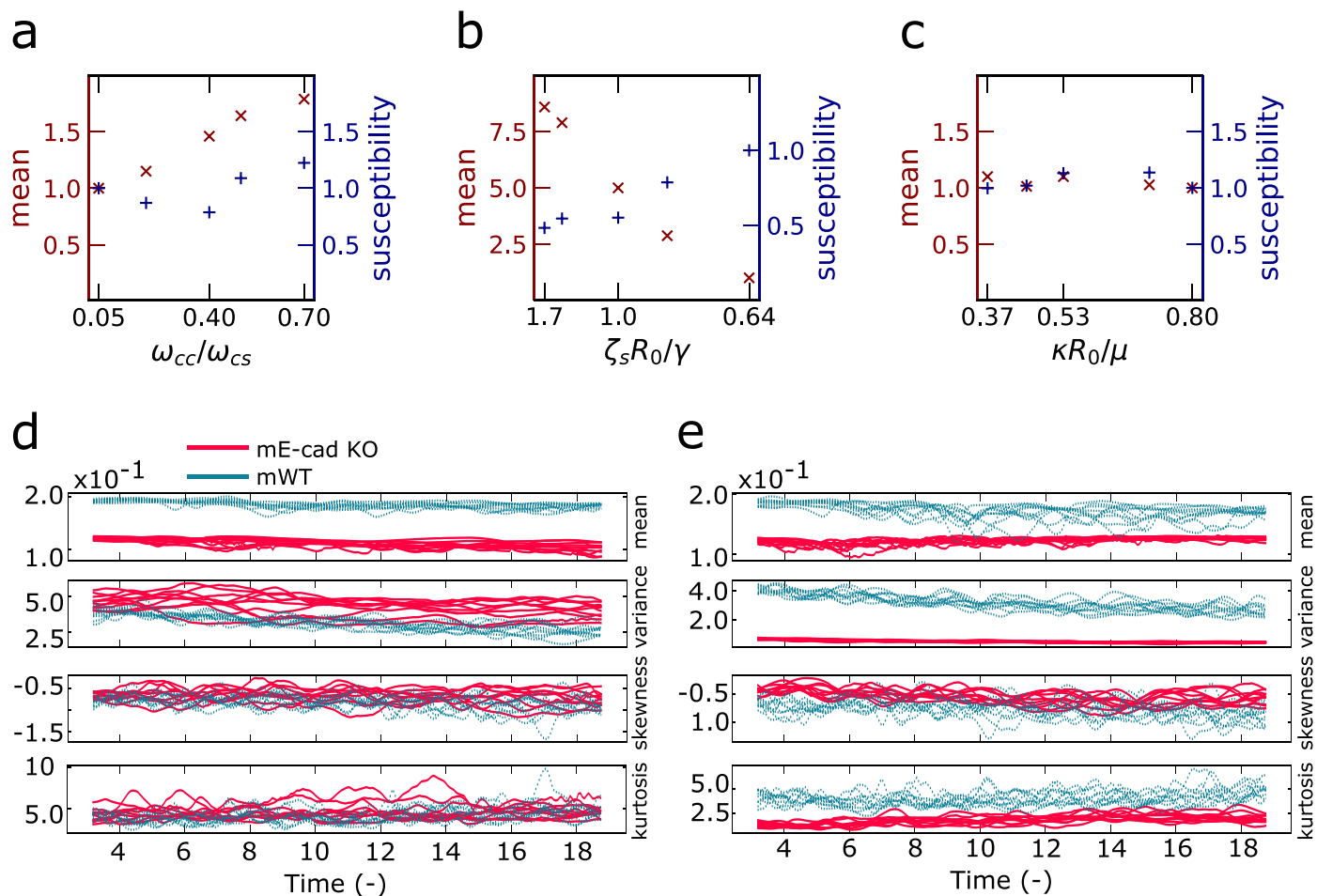
Extended Data Fig. 6 | See next page for caption.

Extended Data Fig. 6 | E-cadherin loss promotes basal cell extrusion.
a) Immunostaining of WT (top) and E-cad KO (bottom) monolayers stained for nuclei (cyan), collagen I (yellow), and paxillin (magenta). Scale: 10μm. Plots on the right show the area and length of focal adhesion quantified from 3 different samples. ****p < 0.0001 through an unpaired t-test and n.s is non significant. **b**) Snapshot from a movie of lifeact GFP (grey) tagged MDCK E-cad KO monolayers stained with Hoescht (nuclei, cyan), annexin (magenta) grown on 2D collagen type I gels (yellow). Position i) and ii) are XZ views through the position i) and ii) labelled on the image. Scale: 10μm. **c**) Immunostaining of MDCK E-cad KO monolayers grown on collagen gels depicting the apical (top) and basal (bottom) planes stained for actin (magenta), collagen (yellow), nuclei (blue). The apical and basal planes were identified through actin staining. **d**) Distribution of the number of apical or basal extrusions from 3 individual samples where error bars represent S.D. Scale bar: 10μm. **e**) Immunostaining of MDCK WT (top) and MDCK E-cad KO (bottom) cysts grown in Matrigel for 10 days, stained for actin (magenta), myosin IIA (white), nuclei (blue) and caspase (green). Arrows indicate extruded cells. Scale: 20μm.

Extended Data Fig. 7 | Model sensitivity to various physical parameters. The field statistics for the computational model: For simulations and exper- iments, the susceptiblity values are normalized by the maximums for WT - apoptotic and mWT, respectively. The sensitivity of the computational model and its dimensionless parameters on isotropic stress fields, characterized by mean and susceptibility, for (**a**) adhesion, (**b**) elasticity and (**c**) compressiblity. The values

are normalized by the bench case, here defined as the lowest for each studied parameter. Time evolution for the global field statistics, characterized by its mean, variance, skewness and kurtosis, to quantify the how elastic contrast between mWT and mE-cad KO cells affects field statistics, (**d**) with no contrast and (**e**) with an elastic contrast. Each curve corresponds to a unique realization for mE-cad KO (solid, red) and mWT (dotted, blue).

Corresponding author(s): Rene-Marc Mege, Amin Doostmohammadi, Benoit Ladoux

Last updated by author(s): Oct 16, 2024

Reporting Summary

Nature Portfolio wishes to improve the reproducibility of the work that we publish. This form provides structure for consistency and transparency in reporting. For further information on Nature Portfolio policies, see our Editorial Policies and the Editorial Policy Checklist.

Statistics

For all statistical analyses, confirm that the following items are present in the figure legend, table legend, main text, or Methods section.

n/a	Confirmed	
☐	☒	The exact sample size (*n*) for each experimental group/condition, given as a discrete number and unit of measurement
☐	☒	A statement on whether measurements were taken from distinct samples or whether the same sample was measured repeatedly
☐	☒	The statistical test(s) used AND whether they are one- or two-sided *Only common tests should be described solely by name; describe more complex techniques in the Methods section.*
☒	☐	A description of all covariates tested
☒	☐	A description of any assumptions or corrections, such as tests of normality and adjustment for multiple comparisons
☐	☒	A full description of the statistical parameters including central tendency (e.g. means) or other basic estimates (e.g. regression coefficient) AND variation (e.g. standard deviation) or associated estimates of uncertainty (e.g. confidence intervals)
☐	☒	For null hypothesis testing, the test statistic (e.g. F, t, r) with confidence intervals, effect sizes, degrees of freedom and *P* value noted *Give P values as exact values whenever suitable.*
☒	☐	For Bayesian analysis, information on the choice of priors and Markov chain Monte Carlo settings
☒	☐	For hierarchical and complex designs, identification of the appropriate level for tests and full reporting of outcomes
☒	☐	Estimates of effect sizes (e.g. Cohen's *d*, Pearson's *r*), indicating how they were calculated

Our web collection on statistics for biologists contains articles on many of the points above.

Software and code

Policy information about availability of computer code

Data collection	Images were collected using Nikon Biostation R, Zeiss 780, and 980 Confocal, Zeiss CSU X1 spinning disk,
Data analysis	Data were analyzed using Python and Matlab

For manuscripts utilizing custom algorithms or software that are central to the research but not yet described in published literature, software must be made available to editors and reviewers. We strongly encourage code deposition in a community repository (e.g. GitHub). See the Nature Portfolio guidelines for submitting code & software for further information.

Data

Policy information about availability of data

All manuscripts must include a data availability statement. This statement should provide the following information, where applicable:
- Accession codes, unique identifiers, or web links for publicly available datasets
- A description of any restrictions on data availability
- For clinical datasets or third party data, please ensure that the statement adheres to our policy

This has been added into the manuscript

Research involving human participants, their data, or biological material

Policy information about studies with human participants or human data. See also policy information about sex, gender (identity/presentation), and sexual orientation and race, ethnicity and racism.

Reporting on sex and gender	*Use the terms sex (biological attribute) and gender (shaped by social and cultural circumstances) carefully in order to avoid confusing both terms. Indicate if findings apply to only one sex or gender; describe whether sex and gender were considered in study design; whether sex and/or gender was determined based on self-reporting or assigned and methods used. Provide in the source data disaggregated sex and gender data, where this information has been collected, and if consent has been obtained for sharing of individual-level data; provide overall numbers in this Reporting Summary. Please state if this information has not been collected. Report sex- and gender-based analyses where performed, justify reasons for lack of sex- and gender-based analysis.*
Reporting on race, ethnicity, or other socially relevant groupings	*Please specify the socially constructed or socially relevant categorization variable(s) used in your manuscript and explain why they were used. Please note that such variables should not be used as proxies for other socially constructed/relevant variables (for example, race or ethnicity should not be used as a proxy for socioeconomic status). Provide clear definitions of the relevant terms used, how they were provided (by the participants/respondents, the researchers, or third parties), and the method(s) used to classify people into the different categories (e.g. self-report, census or administrative data, social media data, etc.) Please provide details about how you controlled for confounding variables in your analyses.*
Population characteristics	*Describe the covariate-relevant population characteristics of the human research participants (e.g. age, genotypic information, past and current diagnosis and treatment categories). If you filled out the behavioural & social sciences study design questions and have nothing to add here, write "See above."*
Recruitment	*Describe how participants were recruited. Outline any potential self-selection bias or other biases that may be present and how these are likely to impact results.*
Ethics oversight	*Identify the organization(s) that approved the study protocol.*

Note that full information on the approval of the study protocol must also be provided in the manuscript.

Field-specific reporting

Please select the one below that is the best fit for your research. If you are not sure, read the appropriate sections before making your selection.

☒ Life sciences   ☐ Behavioural & social sciences   ☐ Ecological, evolutionary & environmental sciences

For a reference copy of the document with all sections, see nature.com/documents/nr-reporting-summary-flat.pdf

Life sciences study design

All studies must disclose on these points even when the disclosure is negative.

Sample size	Sample size used for each case has been specified within the figure legends
Data exclusions	*Describe any data exclusions. If no data were excluded from the analyses, state so OR if data were excluded, describe the exclusions and the rationale behind them, indicating whether exclusion criteria were pre-established.*
Replication	*Describe the measures taken to verify the reproducibility of the experimental findings. If all attempts at replication were successful, confirm this OR if there are any findings that were not replicated or cannot be reproduced, note this and describe why.*
Randomization	*Describe how samples/organisms/participants were allocated into experimental groups. If allocation was not random, describe how covariates were controlled OR if this is not relevant to your study, explain why.*
Blinding	*Describe whether the investigators were blinded to group allocation during data collection and/or analysis. If blinding was not possible, describe why OR explain why blinding was not relevant to your study.*

Reporting for specific materials, systems and methods

We require information from authors about some types of materials, experimental systems and methods used in many studies. Here, indicate whether each material, system or method listed is relevant to your study. If you are not sure if a list item applies to your research, read the appropriate section before selecting a response.

Materials & experimental systems

n/a	Involved in the study
☐	☒ Antibodies
☐	☒ Eukaryotic cell lines
☒	☐ Palaeontology and archaeology
☒	☐ Animals and other organisms
☒	☐ Clinical data
☒	☐ Dual use research of concern
☒	☐ Plants

Methods

n/a	Involved in the study
☒	☐ ChIP-seq
☐	☒ Flow cytometry
☒	☐ MRI-based neuroimaging

Antibodies

Antibodies used	activated caspase-3 (1:200; Sigma Aldrich), Myosin IIA (1:100, Abnova), ZO1 (a gift from Sylvie Robine, 1:20), ppMLC (T18/S19, 3674, cell signaling, 1:100), gp135 (DSHB, 1:20). Anti-mouse, anti-rat and anti-rabbit secondary antibodies conjugated with Alexa (488 or 568; used at 1:200 dilution), Alexa 488 (1:200), Hoescht (1:100) and Alexa 647 (1:50) conjugated phalloidin were purchased from Life Technologies.
Validation	*Describe the validation of each primary antibody for the species and application, noting any validation statements on the manufacturer's website, relevant citations, antibody profiles in online databases, or data provided in the manuscript.*

Eukaryotic cell lines

Policy information about cell lines and Sex and Gender in Research

Cell line source(s)	MDCK WTII and MDCK E-cadherin Knock out cells were used in this study. WT cells were obtained from James Nelson's lab and tested for mycoplasma regularly.. E-cadherin knockout was generated in the lab and published previously in Balasubramaniam et al, Nat Materials, 2021
Authentication	*Describe the authentication procedures for each cell line used OR declare that none of the cell lines used were authenticated.*
Mycoplasma contamination	Cell lines were regularly tested for mycoplasma
Commonly misidentified lines (See ICLAC register)	*Name any commonly misidentified cell lines used in the study and provide a rationale for their use.*

Plants

Seed stocks	*Report on the source of all seed stocks or other plant material used. If applicable, state the seed stock centre and catalogue number. If plant specimens were collected from the field, describe the collection location, date and sampling procedures.*
Novel plant genotypes	*Describe the methods by which all novel plant genotypes were produced. This includes those generated by transgenic approaches, gene editing, chemical/radiation-based mutagenesis and hybridization. For transgenic lines, describe the transformation method, the number of independent lines analyzed and the generation upon which experiments were performed. For gene-edited lines, describe the editor used, the endogenous sequence targeted for editing, the targeting guide RNA sequence (if applicable) and how the editor was applied.*
Authentication	*Describe any authentication procedures for each seed stock used or novel genotype generated. Describe any experiments used to assess the effect of a mutation and, where applicable, how potential secondary effects (e.g. second site T-DNA insertions, mosiacism, off-target gene editing) were examined.*

Flow Cytometry

Plots

Confirm that:

☒ The axis labels state the marker and fluorochrome used (e.g. CD4-FITC).

☒ The axis scales are clearly visible. Include numbers along axes only for bottom left plot of group (a 'group' is an analysis of identical markers).

☒ All plots are contour plots with outliers or pseudocolor plots.

☒ A numerical value for number of cells or percentage (with statistics) is provided.

Methodology

Sample preparation	Detached cells were collected from supernatant and stained with propidium iodide before passing through the cytometer.

Instrument	CyAn ADP (Beckman Coulter) analyser system
Software	FlowJo
Cell population abundance	*Describe the abundance of the relevant cell populations within post-sort fractions, providing details on the purity of the samples and how it was determined.*
Gating strategy	This was determined based on negative controls

☒ Tick this box to confirm that a figure exemplifying the gating strategy is provided in the Supplementary Information.